Universidad de Concepción
Facultad de Ciencias Físicas y Matemáticas
Departamento de Ingeniería Matemática

ACOUSTIC SCATTERING AND ELASTIC WAVES: A HYBRIDIZABLE DISCONTINUOUS GALERKIN APPROACH AND AN INCURSION IN THE METHOD OF FUNDAMENTAL SOLUTIONS

por

Fernando Antonio Artaza Covarrubias

Tesis presentada a la Facultad de Ciencias Físicas y Matemáticas de la Universidad de Concepción para optar al título profesional de Ingeniero Civil Matemático

Profesores Guía: Dr. Manuel Solano Palma (Universidad de Concepción)
Dr. Tonatiuh Sánchez-Vizuet (University of Arizona)

Marzo de 2025
Concepción, Chile.

© 2025 Fernando Antonio Artaza Covarrubias

Se autoriza la reproducción total o parcial, con fines académicos, por cualquier medio o procedimiento, incluyendo la cita bibliográfica del documento.

Evaluation Committee

ACOUSTIC SCATTERING AND ELASTIC WAVES: A HYBRIDIZABLE DISCONTINUOUS GALERKIN APPROACH AND AN INCURSION IN THE METHOD OF FUNDAMENTAL SOLUTIONS

Fernando Antonio Artaza Covarrubias

Dr. Manuel Solano Palma
Universidad de Concepción
Supervisor

Dr. Tonatiuh Sánchez-Vizuet
University of Arizona
Co-Supervisor

Dr. Rommel Bustinza Pariona
Universidad de Concepción
Committee Member

Dr. Bo Dong
University of Massachusetts Dartmouth
Committee Member

Concepción, March 2025.

A mi querida abuelita Florencia Gray Cauquelin, quien, al escuchar la palabra "matemática", sentía que un escalofrío desagradable le recorría la espalda.

Agradecimientos

En primer lugar, quiero agradecer a mis padres, Doris y Andrés, y a mis hermanos, Andrés y Tomás, por todo el apoyo y cariño que siempre me han dado.

En segundo lugar, también quiero expresar mi gratitud a mi profesor guía, Manuel Solano, por haberme aceptado como alumno tesista. Su ayuda, dedicación y calidad humana son realmente invaluables. Le agradezco además la oportunidad de realizar la pasantía en Tucson.

En tercer lugar, a mi profesor co-guía, Tonatiuh Sánchez-Vizuet, quien, a pesar de la distancia, aceptó participar en esta tesis, incluso proponiendo el tema. Gracias por su cálido recibimiento en Tucson y por las interesantes reuniones que tuvimos. También a la profesora Lise-Marie Imbert-Gérard, juntos hicieron que mi experiencia en el desierto fuera muy bonita.

En cuarto lugar, a los buenos profesores que he tenido a lo largo de la carrera. En especial al profesor Raimund Bürger, por su amabilidad y apoyo; al profesor Rommel Bustinza, por su simpatía, cercanía, rigurosidad y por aceptar ser parte de la comisión evaluadora; al profesor Leonardo Figueroa, quien se lleva el premio (o castigo) de haberme hecho la mayor cantidad de asignaturas, gracias por sus interesantes clases y por acogerme durante mi efímera participación en (COPI)^2; al profesor Gabriel Gatica, con quien tuve la dicha de cursar Elementos Finitos Mixtos, gracias por sus buenísimas cátedras y por sus gestiones que me permitieron realizar una pasantía en Vancouver; al profesor Freddy Paiva, por las divertidas conversaciones de pasillo y sus sabios consejos; al profesor Rodolfo Rodríguez, por su interesante electivo y por ser tan auténtico que aun teniendo clases en línea se sentía igual o más cercano que la presencialidad;

y a la profesora Mónica Selva, por su cordialidad y por su respuesta al correo que, al día que escribo estas palabras, hace exactamente ocho años le envié preguntando sobre la carrera, definitivamente parte de que esté aquí es debido a usted. También a los profesores Rodolfo Araya y Dominique Spehner por sus buenas y entretenidas clases.

En quinto lugar, quiero agradecer a los amigos que he encontrado durante este camino. En especial a mis compañeros de batallas numéricas, Luciano Gajardo y Estefanía Olivares, con quienes perfeccioné el arte de la procrastinación, y a todos los demás integrantes de tal grupo cuyo nombre no puedo escribir pues se perdería toda seriedad en este documento: Camila Albornoz, Daniela Castañeda, Bruno Daveggio, Constanza Gacitúa, Annie González, Milene Gutiérrez, Yotán Hidalgo, Nikolas Jara y Ricardo Vega. Gracias por todas esas provechosas jornadas de estudio que duraban hasta un poquito después de que se me empezaran a cerrar los párpados del ojo derecho. A Brayan Sandoval, a quien no solo le quiero dar las gracias por su amistad, sino que también le quiero pedir disculpas por nunca entender de qué me está hablando. A Bastián Flores y Benjamín Mendieta, quienes, junto a Luciano y Ricardo, han evitado (o acelerado, según el día) mi descenso a la locura. Y, en general, a todos los compañeros de la carrera, pues han contribuido a crear un ambiente muy especial y acogedor.

En sexto lugar, quiero agradecer al Centro de Investigación en Ingeniería Matemática (CI^{2}MA) por darme un espacio para trabajar, y en especial a la señora Lorena y a la señora Paola, cuyo trato amable hizo que subir a la cima del cerro siempre se sintiera como volver a casa.

En séptimo lugar, quiero agradecer a todos los estudiantes que tuve en las treinta y un ayudantías que tomé durante mi paso por la carrera, quienes me permitieron realizar una de las actividades que más disfruto en la vida. Gracias por su atención, respeto y por todo lo que me enseñaron.

Finalmente, agradezco a ANID-Chile por su apoyo a través del proyecto Fondecyt Regular 1240183.

Abstract

We are interested in the computational simulation of the interaction between a transient acoustic wave and a bounded elastic solid in an unbounded fluid medium. We start by placing an artificial boundary surrounding the solid, where we impose boundary conditions that do not necessarily represent the physics of the problem. After applying the Laplace transform to the original problem, we propose and analyze a coupled Hybridizable Discontinuous Galerkin (HDG) scheme, in which two mixed variables are included (the stress tensor and the velocity of the acoustic wave) and the symmetry of the stress tensor is imposed weakly by adding the antisymmetric part of the strain tensor (the rotation) as an additional unknown. The optimal convergence of the method is demonstrated theoretically and some preliminary numerical results are presented. In the last chapter, we introduce the Method of Fundamental Solutions and use it to solve some boundary value problems in order to familiarize ourselves with this tool and set the basis to couple the Method of Fundamental Solutions with an HDG scheme in a future work.

Resumen

Estamos interesados en simular computacionalmente la interacción entre una onda acústica transitoria y un sólido elástico acotado en un medio fluido no acotado. Comenzamos colocando una frontera artificial alrededor del sólido, en donde imponemos condiciones de contorno que no necesariamente representan la física del problema. Luego de aplicar la transformada de Laplace al problema original, proponemos y analizamos un esquema de Galerkin Discontinuo Hibridizable (HDG) acoplado, en donde incluimos dos variables mixtas (el tensor de esfuerzos y la velocidad de la onda acústica) y la simetría del tensor de esfuerzos es impuesta débilmente al añadir la parte antisimétrica del tensor de deformaciones (la rotación) como una incógnita adicional. Se demuestra teóricamente que el método HDG acoplado propuesto posee órdenes de convergencia óptimos y se presentan algunos resultados numéricos preliminares. En el último capítulo, introducimos el Método de Soluciones Fundamentales y lo usamos para resolver algunos problemas de valores de contorno con el objetivo de familiarizarnos con esta herramienta y sentar las bases para acoplar el Método de Soluciones Fundamentales con un esquema HDG en un trabajo futuro.

Contents

List of Figures

List of Tables

Introduction

We are interested in the computational simulation of the interaction between a transient acoustic wave and a homogeneous, isotropic and linearly elastic solid. The physical setting of the problem is as follows. An incident acoustic wave v^{inc}—propagating at constant speed c in a homogeneous, isotropic and irrotational fluid with density ρ_f filling a region Ω_A—impinges upon an elastic body of density ρ_E contained in a bounded region Ω_E with Lipschitz boundary Γ and exterior unit normal vector $\boldsymbol{n}_E$. Part of the energy and momentum carried by the acoustic wave is transferred to the elastic solid, exciting an internal elastic wave $\boldsymbol{u}$, while the remaining momentum and energy are carried by an acoustic wave v that is scattered off the surface Γ of the elastic body. Due to the linearity of the problem, the total acoustic wave

$$v^{\mathrm{tot}} = v^{\mathrm{inc}} + v$$

is the superposition of the known incident field v^{inc} and the unknown scattered field v. The unknowns are thus the scattered acoustic field v and the excited elastic displacement field $\boldsymbol{u}$ that satisfy the following system of time-dependent partial differential equations [51]:

$$\begin{aligned}
-\nabla\cdot\left(2\mu\boldsymbol{\varepsilon}\left(\boldsymbol{u}\right)+\lambda\nabla\cdot\boldsymbol{u}\boldsymbol{I}\right)+\rho_E\ddot{\boldsymbol{u}} &= \boldsymbol{f} && \text{in } \Omega_E,\\
-\Delta v+\frac{1}{c^2}\ddot{v} &= f && \text{in } \Omega_A,\\
\nabla v^{\mathrm{tot}}\cdot\boldsymbol{n}_E+\dot{\boldsymbol{u}}\cdot\boldsymbol{n}_E &= 0 && \text{on } \Gamma,\\
\rho_f\dot{v}^{\mathrm{tot}}\boldsymbol{n}_E+\left(2\mu\boldsymbol{\varepsilon}\left(\boldsymbol{u}\right)+\lambda\nabla\cdot\boldsymbol{u}\boldsymbol{I}\right)\boldsymbol{n}_E &= \boldsymbol{0} && \text{on } \Gamma,
\end{aligned}$$

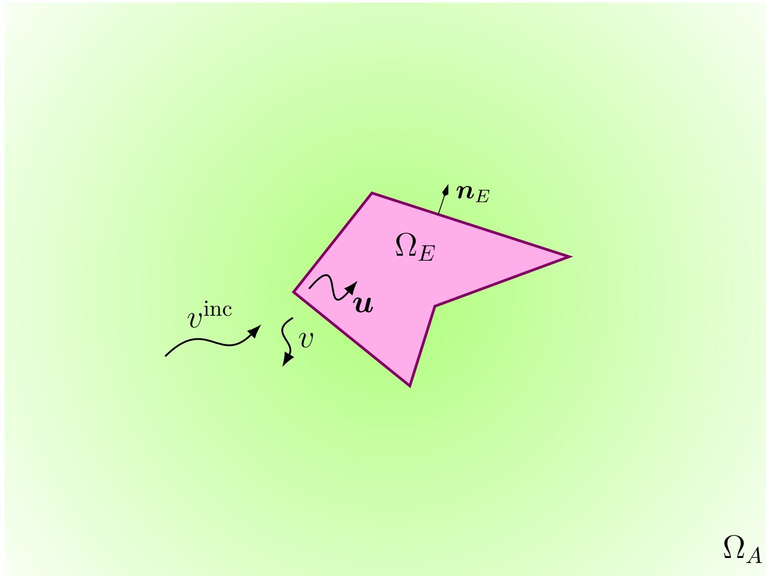

Figure 0.1: Physical setting of the problem.

including suitable initial and radiation conditions, where the upper dot represents differentiation with respect to time, $\boldsymbol{\varepsilon}(\boldsymbol{u}) := \frac{1}{2}(\nabla \boldsymbol{u} + \nabla^{\top} \boldsymbol{u})$ is the strain tensor, $\boldsymbol{I}$ is the identity tensor, $\boldsymbol{f}$ and f are source terms and the Lamé constants, μ (shear modulus) and λ (Lamé's first parameter), encode the material properties of the solid. The physical setting is represented graphically in Figure 0.1.

When viewed in full generality, the acoustic propagation region Ω_A is in fact unbounded and given by $\Omega_A := \mathbb{R}^n \setminus \overline{\Omega_E}$. This fact introduces further computational challenges that are often addressed either through an integral equation representation of the acoustic wave [5, 38, 39, 52], the introduction of a perfectly matched layer [43], the use of absorbing boundary conditions [26, 36, 37, 55] or the representation of the acoustic field through a moment expansion [2].

In Chapter I, we simplify the analysis by assuming that the acoustic domain Ω_A is in fact a bounded region, and boundary conditions ensuring the well-posedness of the problem will be imposed on the exterior boundary Γ_A (see Figure 1.1).

In Chapter II, we present a brief introduction to the Method of Fundamental Solutions, where we will solve some simple problems to familiarize ourselves with this tool. Coupling the Method of Fundamental Solutions with the Hybridizable Discontinuous Galerkin scheme, in order to solve the problem in the unbounded domain, will be a future work.

Chapter 1

A Coupled HDG Discretization for the Interaction Between Acoustic and Elastic Waves

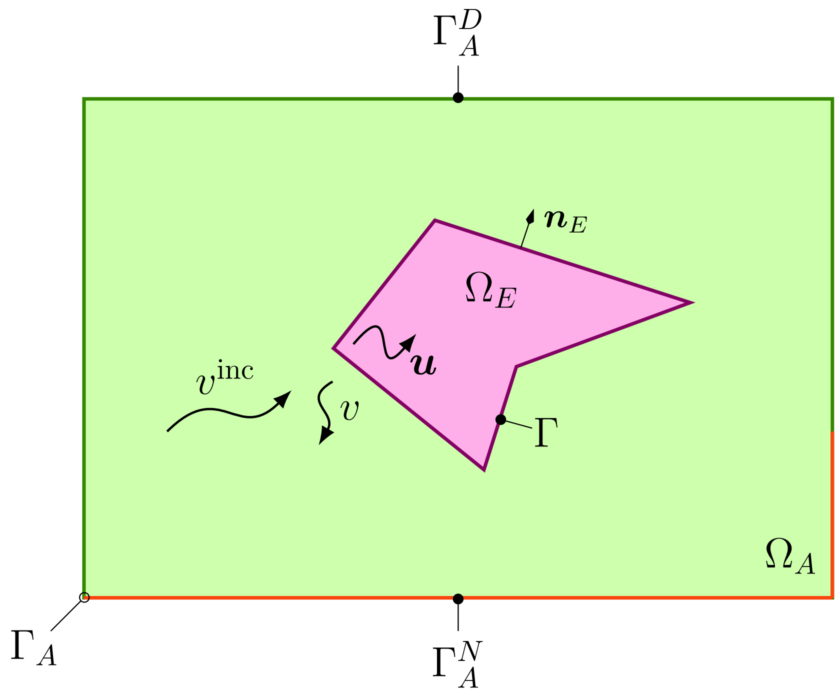

Figure 1.1: Simplified physical setting of the problem.

1.1 Introduction

As mentioned in the introduction, in this memoir we will consider a simplified version of the problem where the acoustic domain Ω_A is bounded and has a polygonal Lipschitz boundary Γ_A (the subscript standing for "artificial") that is divided into mutually disjoint Dirichlet and Neumann segments (respectively Γ_A^D and Γ_A^N) such that $\Gamma_A = \Gamma_A^D \cup \Gamma_A^N$, where appropriate boundary conditions will be prescribed to ensure the well-posedness of the system. We emphasize that the boundary conditions imposed on Γ_A do not attempt to account for a physically outgoing wave; the treatment of the fully unbounded problem will be left for a follow up project. Instead, the goal of this work is to establish the well-posedness theory for the coupling of HDG discretizations for elastic and acoustic wave propagation. This simplified physical setting is shown in Figure 1.1.

Upon Laplace transformation, which maps time differentiation into multiplication by the Laplace parameter $s \in \mathbb{C}$, and using the same symbols for the unknowns in the time domain and in the Laplace domain, the elastic wave $\boldsymbol{u}$ and the scattered acoustic wave v satisfy the coupled system of equations in mixed form

$$\boldsymbol{\sigma} - \mathbf{C}\boldsymbol{\varepsilon}(\boldsymbol{u}) = \mathbf{0} \qquad \text{in } \Omega_E, \tag{1.1a}$$

$$-\nabla\cdot\boldsymbol{\sigma} + \rho_E s^2 \boldsymbol{u} = \boldsymbol{f} \qquad \text{in } \Omega_E, \tag{1.1b}$$

$$\boldsymbol{q} - \nabla v = \mathbf{0} \qquad \text{in } \Omega_A, \tag{1.1c}$$

$$-\nabla\cdot\boldsymbol{q} + (s/c)^2 v = f \qquad \text{in } \Omega_A, \tag{1.1d}$$

$$\boldsymbol{q}\cdot\boldsymbol{n}_A - s\,\boldsymbol{u}\cdot\boldsymbol{n}_E = -\nabla v^{\text{inc}}\cdot\boldsymbol{n}_A \qquad \text{on } \Gamma, \tag{1.1e}$$

$$-\boldsymbol{\sigma}\boldsymbol{n}_E + \rho_f s\, v\, \boldsymbol{n}_A = -\rho_f s\, v^{\text{inc}}\, \boldsymbol{n}_A \qquad \text{on } \Gamma, \tag{1.1f}$$

$$v = g_D \qquad \text{on } \Gamma_A^D, \tag{1.1g}$$

$$\boldsymbol{q}\cdot\boldsymbol{n}_A = g_N \qquad \text{on } \Gamma_A^N. \tag{1.1h}$$

Here, $s \in \{z \in \mathbb{C} : \mathrm{Re}(z) > 0\}$ is the Laplace parameter, $\boldsymbol{u}$ is the unknown displacement, $\boldsymbol{\sigma}$ is the Cauchy stress tensor, $\boldsymbol{f} \in \boldsymbol{L}^2(\Omega_E)$ and $f \in L^2(\Omega_A)$ are source terms, $g_D \in H^{1/2}(\Gamma_A)$ and $g_N \in H^{-1/2}(\Gamma_A)$ are given boundary data. Hooke's elasticity tensor $\mathbf{C}$ is defined by its action on an arbitrary square matrix $\boldsymbol{M}$ as

$$\mathbf{C}\boldsymbol{M} := 2\mu\boldsymbol{M} + \lambda\mathrm{tr}(\boldsymbol{M})\boldsymbol{I} \quad \text{and} \quad \mathbf{C}^{-1}(\boldsymbol{M}) := \frac{1}{2\mu}\boldsymbol{M} - \frac{\lambda}{2\mu(n\lambda + 2\mu)}\mathrm{tr}(\boldsymbol{M})\boldsymbol{I}, \tag{1.2}$$

where, $\boldsymbol{I}$ denotes the identity tensor, and $\mathrm{tr}(\boldsymbol{M}) := \sum_{i=1}^n M_{ii}$, is the matrix trace operator.

In the system above, equations (1.1a) and (1.1b) account for the Navier-Lamé or elastic wave equation in the interior of the elastic solid Ω_E; similarly, equations (1.1c) and (1.1d) are the mixed form of the acoustic wave equation in Ω_A. The elastic and acoustic variables are coupled through the continuity of the normal component of the velocity field across the interface Γ, encoded in equation (1.1e), and the balance of normal forces at the contact surface, given in (1.1f). The nonphysical boundary conditions (1.1g) and (1.1h) prescribed at the artificial boundary Γ_A are given to ensure the well-posedness of the problem. The imposition of the correct outgoing wave boundary conditions will be the subject of subsequent work.

In the literature, there is a vast amount of research related to fluid-structure interaction problems. For instance, some of them use a Mixed Finite Elements approach [25, 31] and there are also couplings of this technique with Boundary Element Methods [30]. Studies on their spectral problems [45] and an analysis of the elastoacustic problem in the time domain [3] have been done. But most of these works assume a time-harmonic regime, so the starting equations change.

Since two different systems of PDEs posed in different domains are being coupled across an interface, we prefer to use a discontinuous Galerkin scheme due to its flexibility to handle the transmission conditions. In particular, by considering the HDG method introduced in [19], it is very easy to impose transmission conditions from the computational point of view. In fact, let us recall that in HDG schemes the only globally coupled degrees of freedom are those of the numerical traces on the boundaries between elements, while the remaining unknowns are obtained by solving local problems in each element. Therefore, if we have two independent HDG solvers, one for the acoustic problem and another one for the elasticity system, we can couple them across the interface through the numerical traces associated with the acoustic wave v and the elastic displacements $\boldsymbol{u}$.

After [19] and the pioneering work [21] that set a framework that simplifies the analysis of a family of HDG schemes by introducing a suitable projection, HDG schemes have been developed for a wide variety of problems. For example, convection-diffusion equation [29, 46], Stokes flow [20, 32]; Brinkman, Oseen and Navier–Stokes equations [9, 10, 28, 48]. In the context of electromagnetism and wave propagation problems, HDG schemes have also been introduced: Maxwell's operator [13, 14], eddy current problems [6], Maxwell's equations in the frequency-domain [27, 47] and heterogeneous media [7] and Helmholtz equation [12, 34, 57]. For the elasticity problem, we refer the reader to [23, 49]. The above list of references is not exhaustive, but provides an overview of the development of HDG schemes during the last fifteen years.

On the other hand, in the context of coupled problems with piecewise linear interfaces, HDG schemes have been proposed for elliptic [40] and for the Stokes interface problems [56], and for Stokes-Darcy coupling [33]. The influence of hanging-nodes along the interface and the use of different polynomial degree over each local space, have been analyzed in [15, 16].

Recently, a new approach has been proposed to handle discrete interfaces that not necessarily coincides with the true interface, as in the case of a curved interface [4, 44, 54] and it is based on the Transfer Path Method [22, 24, 50]. This technique produces a high order method and is closely related with our ultimate goal, where it is crucial to have a numerical scheme that couples an HDG discretization of the problem posed in an bounded domain considering a solid with a curved boundary, and a representation of the acoustic wave in the unbounded region. To the best of our knowledge, the use of HDG schemes has not been analyzed for the coupled problem (1.1), and the main contribution of this work is to provide a convergence analysis.

1.2 Preliminaries and notation

1.2.1 Sobolev spaces.

Let $\mathcal{O}$ be a Lipschitz continuous domain in $\mathbb{R}^n$. We use standard notations for Lebesgue $\mathrm{L}^t(\mathcal{O})$ and Sobolev spaces $\mathrm{W}^{l,t}(\mathcal{O})$, with $l \geq 0$ and $t \in [1, +\infty)$. Here $\mathrm{W}^{0,t}(\mathcal{O}) = \mathrm{L}^t(\mathcal{O})$, and if $t = 2$ we write $\mathrm{H}^l(\mathcal{O})$ instead of $\mathrm{W}^{l,2}(\mathcal{O})$, with the corresponding norm and seminorm denoted by $\|\cdot\|_{H^l(\mathcal{O})}$ and $|\cdot|_{H^l(\mathcal{O})}$, respectively. The spaces of vector-valued functions will be denoted in boldface, therefore $\boldsymbol{H}^s(\mathcal{O}) := [H^s(\mathcal{O})]^n$, whereas for tensor-valued functions, we write $\underline{\boldsymbol{H}}^s(\mathcal{O}) := [H^s(\mathcal{O})]^{n\times n}$. Using the same notation, we write $\boldsymbol{L}^2(\mathcal{O}) := [L^2(\mathcal{O})]^n$ and $\underline{\boldsymbol{L}}^2(\mathcal{O}) := [L^2(\mathcal{O})]^{n\times n}$.

The complex L^2-inner products will be denoted by $(\cdot,\cdot)_{\mathcal{O}}$ and $\langle\cdot,\cdot\rangle_\Sigma$, where Σ is either a Lipschitz curve ($n = 2$) or a surface ($n = 3$). The associated norms will be denoted by $\|\cdot\|_{\mathcal{O}}$ and $\|\cdot\|_\Sigma$.

It is easy to verify that Hooke's tensor satisfies the following inequalities for all $\boldsymbol{\eta} \in \underline{\boldsymbol{L}}^2(\mathcal{O})$:

$$\left(\frac{1}{2\mu} + \frac{n^2\lambda}{2\mu(n\lambda + 2\mu)}\right)^{-1} \|\boldsymbol{\eta}\|^2_{\mathcal{O},\mathbf{C}^{-1}} \leq \|\boldsymbol{\eta}\|^2_{\mathcal{O}} \leq 2\mu\|\boldsymbol{\eta}\|^2_{\mathcal{O},\mathbf{C}^{-1}},$$

$$\|\boldsymbol{\eta}\|^2_{\mathcal{O},\mathbf{C}} \leq (2\mu + n^2\lambda)\|\boldsymbol{\eta}\|^2_{\mathcal{O}},$$

where we denote $\|\cdot\|_{\mathcal{O},\mathbf{C}^{-1}} := (\mathbf{C}^{-1}\cdot,\cdot)^{1/2}_{\mathcal{O}}$ and $\|\cdot\|_{\mathcal{O},\mathbf{C}} := (\mathbf{C}\cdot,\cdot)^{1/2}_{\mathcal{O}}$.

1.2.2 Mesh and mesh-dependent inner products.

Let $\mathcal{T}_A$ and $\mathcal{T}_E$ be two families of regular triangulations of Ω_A and Ω_E, respectively. We will assume that these triangulations are compatible on the common interface Γ and that both are characterized by a common mesh size h in their respective domains. Given an element K, h_K will denote its diameter and $\boldsymbol{n}_K$ its outward unit normal. When there is no confusion, we will simply write $\boldsymbol{n}$ instead of $\boldsymbol{n}_K$. Set $\dagger \in \{A, E\}$, then $\partial\mathcal{T}_\dagger := \{\partial K : K \in \mathcal{T}_\dagger\}$ and let $\mathcal{E}_\dagger$ denote the set of all faces F of all elements $K \in \mathcal{T}_\dagger$. We will also use the following notation for L^2 inner products of scalar-, vector- and tensor-valued functions, respectively, over an integration domain D:

$$(u, v)_D := \int_D u\overline{v}, \qquad (\boldsymbol{u}, \boldsymbol{v})_D = \int_D \boldsymbol{u} \cdot \overline{\boldsymbol{v}}, \qquad (\boldsymbol{M}, \boldsymbol{N})_D = \int_D \boldsymbol{M} : \overline{\boldsymbol{N}},$$

where the overline denotes complex conjugation and the colon ":" is used to denote the Frobenius inner product of matrices

$$\boldsymbol{M} : \boldsymbol{N} := \sum_{i,j=1}^{n} M_{ij} N_{ij}.$$

With this notation we can express the mesh-dependent L^2 inner products as

$$(u, v)_{\mathcal{T}_\dagger} := \sum_{K\in\mathcal{T}_\dagger} (u, v)_K \,, (\boldsymbol{u}, \boldsymbol{v})_{\mathcal{T}_\dagger} := \sum_{K\in\mathcal{T}_\dagger} (\boldsymbol{u}, \boldsymbol{v})_K \,, \quad (\boldsymbol{M}, \boldsymbol{N})_{\mathcal{T}_\dagger} := \sum_{K\in\mathcal{T}_\dagger} (\boldsymbol{M}, \boldsymbol{N})_K \,,$$

along with the inner products over the mesh skeleton

$$\langle u, v\rangle_{\partial\mathcal{T}_\dagger} := \sum_{K\in\mathcal{T}_\dagger} \langle u, v\rangle_{\partial K} \,, \langle \boldsymbol{u}, \boldsymbol{v}\rangle_{\partial\mathcal{T}_\dagger} := \sum_{K\in\mathcal{T}_\dagger} \langle \boldsymbol{u}, \boldsymbol{v}\rangle_{\partial K} \,, \langle \boldsymbol{M}, \boldsymbol{N}\rangle_{\partial\mathcal{T}_\dagger} := \sum_{K\in\mathcal{T}_\dagger} \langle \boldsymbol{M}, \boldsymbol{N}\rangle_{\partial K} \,.$$

We denote the norms induced by these inner products by

$$\|\cdot\|_{\mathcal{T}_\dagger} := \sqrt{(\cdot,\cdot)_{\mathcal{T}_\dagger}} \qquad \text{and} \qquad \|\cdot\|_{\partial\mathcal{T}_\dagger} := \sqrt{\langle\cdot,\cdot\rangle_{\partial\mathcal{T}_\dagger}}.$$

Finally, to avoid proliferation of unimportant constants, we will write $a \lesssim b$ when there exists a positive constant C, independent of the meshsize, such that $a \leq Cb$.

1.3 An HDG discretization

For the Navier-Lamé equations (1.1a)-(1.1b), we will follow the approach from [23], where the symmetry of the stress tensor is imposed weakly by introducing the spin tensor

$$\boldsymbol{\gamma}(\boldsymbol{u}) := (\nabla \boldsymbol{u} - \nabla^\top \boldsymbol{u})/2$$

as an additional unknown. In this setting, (1.1a) can be written as

$$\mathbf{C}^{-1}\boldsymbol{\sigma} - \nabla \boldsymbol{u} + \boldsymbol{\gamma} = \mathbf{0} \quad \text{in } \Omega_E. \tag{1.3a}$$

For the acoustic equations (1.1c)-(1.1d), we will consider a standard HDG discretization as in [21]. Let us begin by introducing the notation associated with the discretization of the domain, we will then specify the finite-dimensional spaces, and then formulate the HDG scheme.

We will make use of the discrete spaces for the HDG method proposed in [23] for simplices. For an element $K \in \mathcal{T}_A \cup \mathcal{T}_E$, we define the following function spaces. The set of scalar-valued polynomials of degree at most k defined over K will be denoted by $\mathcal{P}_k(K)$, while the corresponding vector and tensor product spaces are denoted respectively as

$$\boldsymbol{\mathcal{P}}_k(K) := [\mathcal{P}_k(K)]^n \qquad \text{and} \qquad \underline{\boldsymbol{\mathcal{P}}}_k(K) := [\mathcal{P}_k(K)]^{n\times n}.$$

The polynomial spaces of degree *exactly* k will be denoted with a tilde as $\widetilde{\mathcal{P}}_k(K)$, $\widetilde{\boldsymbol{\mathcal{P}}}_k(K)$, and $\widetilde{\underline{\boldsymbol{\mathcal{P}}}}_k(K)$. We now define

$$A_{ij}(K) := \begin{cases} \mathcal{P}_k(K) & \text{if } \; i \neq j, \\ 0 & \text{if } \; i = j, \end{cases},$$

and use it to construct the matrix-valued space

$$\underline{\boldsymbol{A}}(K) := [A_{ij}(K)]^{n\times n}.$$

We will denote the space of L^2 integrable skew-symmetric matrices over K by

$$\underline{\boldsymbol{AS}}(K) := \{\boldsymbol{M} \in \underline{\boldsymbol{L}}^2(K) : \boldsymbol{M} + \boldsymbol{M}^\top = \mathbf{0}\},$$

and will require that $\underline{\boldsymbol{A}}(K) \subset \underline{\boldsymbol{AS}}(K)$.

Now, we would like to define a divergence-free space of functions through the use of bubble matrices or bubble scalars, depending on the dimension, as in [18, 8, 23, 35]. Let us define what a bubble matrix is ([35]): A matrix-valued function $\boldsymbol{b}$ defined in Ω_E is said to be an admissible bubble matrix if for each $K \in \mathcal{T}_E$ the matrix $\boldsymbol{b}_K := \boldsymbol{b}|_K$ is a matrix with polynomial entries that satisfies

1. The tangential components of each row of $\boldsymbol{b}_K$ vanish on all the faces of K,
2. There exists $C_1 > 0$ such that $C_1(\boldsymbol{v}, \boldsymbol{v})_K \leq (\boldsymbol{v}\boldsymbol{b}_K, \boldsymbol{v})_K$, for all $\boldsymbol{v} \in \underline{\boldsymbol{L}}^2(K)$,
3. There exists $C_2 > 0$ such that $\|\boldsymbol{b}_K\|_{\underline{\boldsymbol{L}}^\infty(K)} \leq C_2$,

where the constants C_1 and C_2 depend only on the shape regularity of $\mathcal{T}_E$.

Thus, following [18, 23], if η_F is the barycentric coordinate associated to the edge F of K, and if we define

$$\boldsymbol{b}_K := \begin{cases} \displaystyle\prod_{F \subset \partial K} \eta_F & \text{in 2D ,} \\ \displaystyle\sum_{F \subset \partial K} \left[\prod_{F' \subset \partial K \setminus \{F\}} \eta_{F'} \right] \nabla \eta_F \otimes \nabla \eta_F & \text{in 3D,} \end{cases}$$

the polynomial space $\underline{\boldsymbol{B}}(K)$ associated to bubble functions is defined as:

$$\underline{\boldsymbol{B}}(K) := \nabla \times ((\nabla \times \underline{\boldsymbol{A}}(K))\boldsymbol{b}_K).$$

We can observe that any function

$$\boldsymbol{v} \in \underline{\boldsymbol{\mathcal{B}}}_h := \{\boldsymbol{\eta} \in \underline{\boldsymbol{L}}^2(\Omega_E) : \boldsymbol{\eta}|_K \in \underline{\boldsymbol{B}}(K)\,, K \in \mathcal{T}_E\}$$

is such that

$$\nabla \cdot \boldsymbol{v}|_K = 0, \forall\, K \in \mathcal{T}_E \quad \text{ and } \quad \boldsymbol{v}\boldsymbol{n}|_F = 0, \forall F \in \mathcal{E}_E.$$

In the three-dimensional case the curl operator acts row-wise, while in the two-dimensional case the curl of matrices and column vectors are defined respectively by

$$\nabla \times \begin{pmatrix} M_{11} & M_{12} \\ M_{21} & M_{22} \end{pmatrix} := \begin{pmatrix} \partial_x M_{12} - \partial_y M_{11} \\ \partial_x M_{22} - \partial_y M_{21} \end{pmatrix} \quad \text{and} \quad \nabla \times \begin{pmatrix} m_1 \\ m_2 \end{pmatrix} := \begin{pmatrix} -\partial_y m_1 & \partial_x m_1 \\ -\partial_y m_2 & \partial_x m_2 \end{pmatrix}$$

We will also make use of the local space $\underline{\boldsymbol{V}}(K) := \underline{\boldsymbol{\mathcal{P}}}_k(K) + \underline{\boldsymbol{B}}(K)$, and notice that

$$\underline{\boldsymbol{V}}(K) = \underline{\boldsymbol{\mathcal{P}}}_k(K) + \nabla \times ((\nabla \times \underline{\boldsymbol{A}}(K))\boldsymbol{b}_K) = \underline{\boldsymbol{\mathcal{P}}}_k(K) \oplus \nabla \times ((\nabla \times \widetilde{\underline{\boldsymbol{A}}}(K))\boldsymbol{b}_K),$$

where $\widetilde{\underline{\boldsymbol{A}}}(K) := \underline{\boldsymbol{A}}(K) \cap \widetilde{\underline{\boldsymbol{\mathcal{P}}}}_k(K)$.

Finally, we define the piecewise polynomial spaces

$$\underline{\boldsymbol{V}}_h = \{\boldsymbol{\tau} \in \underline{\boldsymbol{L}}^2(\mathcal{T}_E) : \boldsymbol{\tau}|_K \in \underline{\boldsymbol{V}}(K), \quad \forall K \in \mathcal{T}_E\}, \tag{1.4a}$$

$$\boldsymbol{W}_h^E = \{\boldsymbol{t} \in \boldsymbol{L}^2(\mathcal{T}_E) : \boldsymbol{t}|_K \in \boldsymbol{\mathcal{P}}_k(K), \quad \forall K \in \mathcal{T}_E\}, \tag{1.4b}$$

$$\underline{\boldsymbol{A}}_h = \{\boldsymbol{\eta} \in \underline{\boldsymbol{L}}^2(\mathcal{T}_E) : \boldsymbol{\eta}|_K \in \underline{\boldsymbol{A}}(K), \quad \forall K \in \mathcal{T}_E\}, \tag{1.4c}$$

$$\boldsymbol{M}_h = \{\boldsymbol{\mu} \in \boldsymbol{L}^2(\mathcal{E}_E) : \boldsymbol{\mu}|_F \in \boldsymbol{\mathcal{P}}_k(F), \quad \forall F \in \mathcal{E}_E\}, \tag{1.4d}$$

$$\boldsymbol{W}_h^A = \{\boldsymbol{r} \in \boldsymbol{L}^2(\mathcal{T}_A) : \boldsymbol{r}|_K \in \boldsymbol{\mathcal{P}}_k(K), \quad \forall K \in \mathcal{T}_A\}, \tag{1.4e}$$

$$W_h = \{w \in L^2(\mathcal{T}_A) : w|_K \in \mathcal{P}_k(K), \quad \forall K \in \mathcal{T}_A\}, \tag{1.4f}$$

$$M_h = \{\xi \in L^2(\mathcal{E}_A) : \xi|_F \in \mathcal{P}_k(F), \quad \forall F \in \mathcal{E}_A\}, \tag{1.4g}$$

The method seeks a piecewise polynomial approximation

$$(\boldsymbol{\sigma}_h, \boldsymbol{u}_h, \boldsymbol{\gamma}_h, \widehat{\boldsymbol{u}}_h, \boldsymbol{q}_h, v_h, \widehat{v}_h) \in \underline{\boldsymbol{V}}_h \times \boldsymbol{W}_h^E \times \underline{\boldsymbol{A}}_h \times \boldsymbol{M}_h \times \boldsymbol{W}_h^A \times W_h \times M_h$$

of the exact solution $(\boldsymbol{\sigma}, \boldsymbol{u}, \boldsymbol{\gamma}, \boldsymbol{u}|_{\mathcal{E}_E}, \boldsymbol{q}, v, v|_{\mathcal{E}_A})$. The approximation must satisfy the discrete weak formulation

$$(\mathbf{C}^{-1}\boldsymbol{\sigma}_h, \boldsymbol{\tau})_{\mathcal{T}_E} + (\boldsymbol{u}_h, \nabla \cdot \boldsymbol{\tau})_{\mathcal{T}_E} + (\boldsymbol{\gamma}_h, \boldsymbol{\tau})_{\mathcal{T}_E} - \langle \widehat{\boldsymbol{u}}_h, \boldsymbol{\tau}\boldsymbol{n}\rangle_{\partial\mathcal{T}_E} = 0, \tag{1.5a}$$

$$(\boldsymbol{\sigma}_h, \nabla \boldsymbol{t})_{\mathcal{T}_E} - \langle \widehat{\boldsymbol{\sigma}}_h \boldsymbol{n}, \boldsymbol{t}\rangle_{\partial\mathcal{T}_E} + \rho_E s^2 (\boldsymbol{u}_h, \boldsymbol{t})_{\mathcal{T}_E} = (\boldsymbol{f}, \boldsymbol{t})_{\mathcal{T}_E}, \tag{1.5b}$$

$$(\boldsymbol{\sigma}_h, \boldsymbol{\eta})_{\mathcal{T}_E} = 0, \tag{1.5c}$$

$$\langle \widehat{\boldsymbol{\sigma}}_h \boldsymbol{n}, \boldsymbol{\mu}\rangle_{\partial\mathcal{T}_E \setminus \Gamma} = 0, \tag{1.5d}$$

$$(\boldsymbol{q}_h, \boldsymbol{r})_{\mathcal{T}_A} + (v_h, \nabla \cdot \boldsymbol{r})_{\mathcal{T}_A} - \langle \widehat{v}_h, \boldsymbol{r} \cdot \boldsymbol{n}\rangle_{\partial\mathcal{T}_A} = 0, \tag{1.5e}$$

$$(\boldsymbol{q}_h, \nabla w)_{\mathcal{T}_A} - \langle \widehat{\boldsymbol{q}}_h \cdot \boldsymbol{n}, w\rangle_{\partial\mathcal{T}_A} + (s/c)^2 (v_h, w)_{\mathcal{T}_A} = (f, w)_{\mathcal{T}_A}, \tag{1.5f}$$

$$\langle \widehat{\boldsymbol{q}}_h \cdot \boldsymbol{n}, \xi\rangle_{\partial\mathcal{T}_A \setminus (\Gamma \cup \Gamma_A^D)} = \langle g_N, \xi\rangle_{\Gamma_A^N}, \tag{1.5g}$$

$$\langle \widehat{v}_h, \xi \rangle_{\Gamma_A^D} = \langle g_D, \xi \rangle_{\Gamma_A^D}, \tag{1.5h}$$

$$\langle \widehat{\boldsymbol{q}}_h \cdot \boldsymbol{n}_A - s\, \widehat{\boldsymbol{u}}_h \cdot \boldsymbol{n}_E, \xi \rangle_\Gamma = -\langle \nabla v^{\text{inc}} \cdot \boldsymbol{n}_A, \xi \rangle_\Gamma, \tag{1.5i}$$

$$\langle -\widehat{\boldsymbol{\sigma}}_h \boldsymbol{n}_E + \rho_f s\, \widehat{v}_h\, \boldsymbol{n}_A, \boldsymbol{\mu} \rangle_\Gamma = -\rho_f s\, \langle v^{\text{inc}}\, \boldsymbol{n}_A, \boldsymbol{\mu} \rangle_\Gamma \tag{1.5j}$$

for all test functions $(\boldsymbol{\tau}, \boldsymbol{t}, \boldsymbol{\eta}, \boldsymbol{\mu}, \boldsymbol{r}, w, \xi) \in \underline{\boldsymbol{V}}_h \times \boldsymbol{W}_h^E \times \underline{\boldsymbol{A}}_h \times \boldsymbol{M}_h \times \boldsymbol{W}_h^A \times W_h \times M_h$, where

$$\widehat{\boldsymbol{\sigma}}_h \boldsymbol{n} := \boldsymbol{\sigma}_h \boldsymbol{n} - \tau_E (\boldsymbol{u}_h - \widehat{\boldsymbol{u}}_h) \qquad \text{on} \quad \partial \mathcal{T}_E, \tag{1.5k}$$

$$\widehat{\boldsymbol{q}}_h \cdot \boldsymbol{n} := \boldsymbol{q}_h \cdot \boldsymbol{n} - \tau_A (v_h - \widehat{v}_h) \qquad \text{on} \quad \partial \mathcal{T}_A. \tag{1.5l}$$

Here, τ_E and τ_A are stabilization parameters whose properties will be determined when analyzing the scheme.

1.4 Analysis of the HDG scheme

1.4.1 Well-posedness.

Theorem 1. *If* $\mathrm{Re}(s\tau_A) > 0$ *and* $\mathrm{Re}(s\tau_E) > 0$*, then the scheme* (1.5) *has a unique solution.*

Proof. By the Fredholm alternative, it is enough to show uniqueness of the solution. To that end, if we assume zero sources, we will show that the solution to the corresponding system is the trivial one.

Let

$$v^{\text{inc}} = 0 \quad \text{and} \quad (f, \boldsymbol{f}, g_D, g_N) = (0, \boldsymbol{0}, 0, 0)$$

and choose

$$(\boldsymbol{\tau}, \boldsymbol{t}, \boldsymbol{\eta}, \boldsymbol{\mu}, \boldsymbol{r}, w) = (\widehat{\boldsymbol{\sigma}}_h, \boldsymbol{u}_h, \boldsymbol{\gamma}_h, \widehat{\boldsymbol{u}}_h, \boldsymbol{q}_h, v_h) \quad \text{and} \quad \xi = \begin{cases} \widehat{v}_h, & \text{on } \partial\mathcal{T}_A \setminus \Gamma_A^D \\ \widehat{\boldsymbol{q}}_h \cdot \boldsymbol{n}, & \text{on } \Gamma_A^D \end{cases}.$$

With this choice of test functions, applying integration by parts to (1.5b) and adding its conjugate to (1.5a) we obtain

$$(\mathbf{C}^{-1} \boldsymbol{\sigma}_h, \boldsymbol{\sigma}_h)_{\mathcal{T}_E} + (\boldsymbol{u}_h, \nabla \cdot \boldsymbol{\sigma}_h)_{\mathcal{T}_E} + (\boldsymbol{\gamma}_h, \boldsymbol{\sigma}_h)_{\mathcal{T}_E} - \langle \widehat{\boldsymbol{u}}_h, \boldsymbol{\sigma}_h \boldsymbol{n} \rangle_{\partial \mathcal{T}_E}$$

$$- \overline{(\nabla\cdot\boldsymbol{\sigma}_h, \boldsymbol{u}_h)_{\mathcal{T}_E}} + \overline{\langle\boldsymbol{\sigma}_h\boldsymbol{n}, \boldsymbol{u}_h\rangle_{\partial\mathcal{T}_E}} - \overline{\langle\widehat{\boldsymbol{\sigma}}_h\boldsymbol{n}, \boldsymbol{u}_h\rangle_{\partial\mathcal{T}_E}} + \rho_E\overline{s^2}(\boldsymbol{u}_h, \boldsymbol{u}_h)_{\mathcal{T}_E} = 0.$$

We know from (1.5c) that $(\boldsymbol{\sigma}_h, \boldsymbol{\gamma}_h)_{\mathcal{T}_E} = 0$, so the latter equation becomes

$$(\mathbf{C}^{-1}\boldsymbol{\sigma}_h, \boldsymbol{\sigma}_h)_{\mathcal{T}_E} + \overline{\langle\boldsymbol{\sigma}_h\boldsymbol{n} - \widehat{\boldsymbol{\sigma}}_h\boldsymbol{n}, \boldsymbol{u}_h\rangle_{\partial\mathcal{T}_E}} - \langle\widehat{\boldsymbol{u}}_h, \boldsymbol{\sigma}_h\boldsymbol{n}\rangle_{\partial\mathcal{T}_E} + \rho_E\overline{s^2}(\boldsymbol{u}_h, \boldsymbol{u}_h)_{\mathcal{T}_E} = 0.$$

Adding and subtracting $\widehat{\boldsymbol{u}}_h$ in the second argument of the second term, we have that

$$\begin{aligned}\|\boldsymbol{\sigma}_h\|^2_{\mathcal{T}_E,\mathbf{C}^{-1}} + \overline{\langle\boldsymbol{\sigma}_h\boldsymbol{n} - \widehat{\boldsymbol{\sigma}}_h\boldsymbol{n}, \boldsymbol{u}_h - \widehat{\boldsymbol{u}}_h\rangle_{\partial\mathcal{T}_E}} + \overline{\langle\boldsymbol{\sigma}_h\boldsymbol{n} - \widehat{\boldsymbol{\sigma}}_h\boldsymbol{n}, \widehat{\boldsymbol{u}}_h\rangle_{\partial\mathcal{T}_E}}& \\ - \langle\widehat{\boldsymbol{u}}_h, \boldsymbol{\sigma}_h\boldsymbol{n}\rangle_{\partial\mathcal{T}_E} + \rho_E\overline{s^2}\,\|\boldsymbol{u}_h\|^2_{\mathcal{T}_E} = 0.&\end{aligned}$$

Multiplying by s and using (1.5d), along with the definition (1.5k), we obtain

$$s\,\|\boldsymbol{\sigma}_h\|^2_{\mathcal{T}_E,\mathbf{C}^{-1}} + s\overline{\langle\tau_E(\boldsymbol{u}_h - \widehat{\boldsymbol{u}}_h), \boldsymbol{u}_h - \widehat{\boldsymbol{u}}_h\rangle_{\partial\mathcal{T}_E}} - s\langle\widehat{\boldsymbol{u}}_h, \widehat{\boldsymbol{\sigma}}_h\boldsymbol{n}_E\rangle_\Gamma + \rho_E\overline{s}|s|^2\,\|\boldsymbol{u}_h\|^2_{\mathcal{T}_E} = 0. \tag{1.6}$$

Analogously for the acoustic terms, (1.5f) is integrated by parts and its conjugate is added to (1.5e), yielding

$$\begin{aligned}\|\boldsymbol{q}_h\|^2_{\mathcal{T}_A} + (v_h, \nabla\cdot\boldsymbol{q}_h)_{\mathcal{T}_A} - \langle v_h, \boldsymbol{q}_h\cdot\boldsymbol{n}\rangle_{\partial\mathcal{T}_A} - \overline{(\nabla\cdot\boldsymbol{q}_h, v_h)_{\mathcal{T}_A}}& \\ + \overline{\langle\boldsymbol{q}_h\cdot\boldsymbol{n}, v_h\rangle_{\partial\mathcal{T}_A}} - \overline{\langle\widehat{\boldsymbol{q}}_h\cdot\boldsymbol{n}, v_h\rangle_{\partial\mathcal{T}_A}} + \frac{\overline{s^2}}{c^2}\,\|v_h\|^2_{\mathcal{T}_A} = 0.&\end{aligned}$$

Adding and subtracting $\widehat{v}_h$ and using (1.5g) and (1.5h), we can deduce that

$$\|\boldsymbol{q}_h\|^2_{\mathcal{T}_A} + \overline{\langle\tau_A(v_h - \widehat{v}_h), v_h - \widehat{v}_h\rangle_{\partial\mathcal{T}_A}} - \langle\widehat{v}_h, \widehat{\boldsymbol{q}}_h\cdot\boldsymbol{n}_A\rangle_\Gamma + \frac{\overline{s^2}}{c^2}\,\|v_h\|^2_{\mathcal{T}_A} = 0.$$

We multiply the latter equation by $\rho_f s$ to obtain

$$\rho_f s\,\|\boldsymbol{q}_h\|^2_{\mathcal{T}_A} + \rho_f s\overline{\langle\tau_A(v_h - \widehat{v}_h), v_h - \widehat{v}_h\rangle_{\partial\mathcal{T}_A}} - \rho_f s\langle\widehat{v}_h, \widehat{\boldsymbol{q}}_h\cdot\boldsymbol{n}_A\rangle_\Gamma + \rho_f\overline{s}(|s|/c)^2\,\|v_h\|^2_{\mathcal{T}_A} = 0. \tag{1.7}$$

Adding (1.6) with the conjugate of (1.7) leads to

$$\begin{aligned}s\,\|\boldsymbol{\sigma}_h\|^2_{\mathcal{T}_E,\mathbf{C}^{-1}} + s\overline{\langle\tau_E(\boldsymbol{u}_h - \widehat{\boldsymbol{u}}_h), \boldsymbol{u}_h - \widehat{\boldsymbol{u}}_h\rangle_{\partial\mathcal{T}_E}} - s\langle\widehat{\boldsymbol{u}}_h, \widehat{\boldsymbol{\sigma}}_h\boldsymbol{n}_E\rangle_\Gamma + \rho_E\overline{s}|s|^2\,\|\boldsymbol{u}_h\|^2_{\mathcal{T}_E}& \\ +\rho_f\overline{s}\,\|\boldsymbol{q}_h\|^2_{\mathcal{T}_A} + \rho_f\overline{s}\langle\tau_A(v_h - \widehat{v}_h), v_h - \widehat{v}_h\rangle_{\partial\mathcal{T}_A} - \rho_f\overline{s}\overline{\langle\widehat{v}_h, \widehat{\boldsymbol{q}}_h\cdot\boldsymbol{n}_A\rangle_\Gamma} + \rho_f\overline{s}(|s|/c)^2\,\|v_h\|^2_{\mathcal{T}_A} = 0&\end{aligned} \tag{1.8}$$

Notice that from (1.5i) and (1.5j) we have

$$-s\langle\widehat{\boldsymbol{u}}_h, \widehat{\boldsymbol{\sigma}}_h\boldsymbol{n}_E\rangle_\Gamma - \rho_f\overline{s}\overline{\langle\widehat{v}_h, \widehat{\boldsymbol{q}}_h\cdot\boldsymbol{n}_A\rangle_\Gamma} = -\,s\langle\widehat{\boldsymbol{u}}_h, \widehat{\boldsymbol{\sigma}}_h\boldsymbol{n}_E - \rho_f s\widehat{v}_h\boldsymbol{n}_A\rangle_\Gamma - s\langle\widehat{\boldsymbol{u}}_h, \rho_f s\widehat{v}_h\boldsymbol{n}_A\rangle_\Gamma$$

$$
\begin{aligned}
&-\rho_f\overline{s}\overline{\langle \widehat{v}_h, \widehat{\boldsymbol{q}}_h\cdot \boldsymbol{n}_A - s\widehat{\boldsymbol{u}}_h\cdot \boldsymbol{n}_E\rangle_\Gamma} - \rho_f\overline{s}\overline{\langle \widehat{v}_h, s\widehat{\boldsymbol{u}}_h\cdot \boldsymbol{n}_E\rangle_\Gamma}\\
=&-s\langle \widehat{\boldsymbol{u}}_h, \rho_f s\widehat{v}_h\boldsymbol{n}_A\rangle_\Gamma - \rho_f\overline{s}\overline{\langle \widehat{v}_h, s\widehat{\boldsymbol{u}}_h\cdot \boldsymbol{n}_E\rangle_\Gamma}\\
=&-s\overline{s}\rho_f\langle \widehat{\boldsymbol{u}}_h, \widehat{v}_h\boldsymbol{n}_A\rangle_\Gamma + s\overline{s}\rho_f\langle \widehat{\boldsymbol{u}}_h, \widehat{v}_h\boldsymbol{n}_A\rangle_\Gamma = 0.
\end{aligned}
$$

So, (1.8) is equivalent to

$$
\begin{aligned}
s\left\|\boldsymbol{\sigma}_h\right\|^2_{\mathcal{T}_E,\mathbf{C}^{-1}} + s\overline{\langle \tau_E(\boldsymbol{u}_h-\widehat{\boldsymbol{u}}_h), \boldsymbol{u}_h-\widehat{\boldsymbol{u}}_h\rangle_{\partial\mathcal{T}_E}} + \rho_E\overline{s}|s|^2\left\|\boldsymbol{u}_h\right\|^2_{\mathcal{T}_E}\\
+\rho_f\overline{s}\left\|\boldsymbol{q}_h\right\|^2_{\mathcal{T}_A} + \rho_f\overline{s}\langle \tau_A(v_h-\widehat{v}_h), v_h-\widehat{v}_h\rangle_{\partial\mathcal{T}_A} + \rho_f s(|s|/c)^2\left\|v_h\right\|^2_{\mathcal{T}_A} = 0.
\end{aligned}
$$

Thus, taking real part of this expression, we obtain

$$
\mathscr{E}_E^2 + \mathscr{E}_A^2 + \rho_E|s|^2\mathrm{Re}(s)\left\|\boldsymbol{u}_h\right\|^2_{\mathcal{T}_E} + \frac{\rho_f}{c^2}|s|^2\mathrm{Re}(s)\left\|v_h\right\|^2_{\mathcal{T}_A} = 0\,,
$$

where we have defined

$$
\begin{aligned}
\mathscr{E}_E &:= \sqrt{\left\|\mathrm{Re}(s)^{1/2}\,\boldsymbol{\sigma}_h\right\|^2_{\mathcal{T}_E,\mathbf{C}^{-1}} + \left\|\mathrm{Re}(s\tau_E)^{1/2}\,(\boldsymbol{u}_h-\widehat{\boldsymbol{u}}_h)\right\|^2_{\partial\mathcal{T}_E}}\\
\mathscr{E}_A &:= \sqrt{\left\|\rho_f^{1/2}\mathrm{Re}(s)^{1/2}\,\boldsymbol{q}_h\right\|^2_{\mathcal{T}_A} + \left\|\rho_f^{1/2}\mathrm{Re}(s\tau_A)^{1/2}\,(v_h-\widehat{v}_h)\right\|^2_{\partial\mathcal{T}_A}}.
\end{aligned}
$$

From here, we can conclude that $\boldsymbol{\sigma}_h = \mathbf{0}$ in $\mathcal{T}_E$, $\boldsymbol{u}_h = \mathbf{0}$ in $\mathcal{T}_E$, $\boldsymbol{q}_h = \mathbf{0}$ in $\mathcal{T}_A$, $v_h = 0$ in $\mathcal{T}_A$, $\widehat{\boldsymbol{u}}_h = \boldsymbol{u}_h = \mathbf{0}$ on $\partial\mathcal{T}_E$ and $\widehat{v}_h = v_h = 0$ on $\partial\mathcal{T}_A$.

It only remains to show that $\boldsymbol{\gamma}_h = \mathbf{0}$ in $\mathcal{T}_E$. This will be achieved by performing an analog of the steps done in the proof of [8, Lemma 3.6]. We will need the two following technical results proven in [35]:

1. [35, Lemma 2.8] Given $\boldsymbol{\eta} \in \underline{\boldsymbol{A}}_h^0 := \{\boldsymbol{\eta} \in \underline{\boldsymbol{A}}_h : (\boldsymbol{\eta}, \boldsymbol{v})_K = 0, \forall \boldsymbol{v} \in \underline{\boldsymbol{\mathcal{P}}}_0(K)\,, \forall K \in \mathcal{T}_E\}$, there exists $\boldsymbol{v} \in \underline{\boldsymbol{\mathcal{B}}}_h$ such that

   $$
   \boldsymbol{P}\boldsymbol{v} = \boldsymbol{\eta} \quad \text{and} \quad \left\|\boldsymbol{v}\right\|_{\mathcal{T}_E} \leq C^0\left\|\boldsymbol{\eta}\right\|_{\mathcal{T}_E}.
   $$

   Here $\boldsymbol{P} : \underline{\boldsymbol{L}}^2(\Omega_E) \to \underline{\boldsymbol{A}}_h$ is the L^2-projection onto $\underline{\boldsymbol{A}}_h$ and C^0 is a positive constant independent of h, arising from a Poincaré-type inequality and inverse estimates.

2. [35, Proposition 2.9] Given $\boldsymbol{\eta} \in \underline{\boldsymbol{A}}_h^c := \underline{\boldsymbol{A}}_h \cap \underline{\boldsymbol{\mathcal{P}}}_0(\mathcal{T}_E)$, there exists $\boldsymbol{v} \in \underline{\boldsymbol{H}}(\mathrm{div};\Omega_E) \cap \underline{\boldsymbol{\mathcal{P}}}_1(\mathcal{T}_E)$ such that

$$\nabla \cdot \boldsymbol{v} = 0\,, \qquad \boldsymbol{P}^c \boldsymbol{v} = \boldsymbol{\eta}\,, \qquad \text{and} \qquad \|\boldsymbol{v}\|_{\mathcal{T}_E} = C^c\,\|\boldsymbol{\eta}\|_{\mathcal{T}_E}\,, \tag{1.9}$$

where $\boldsymbol{P}^c$ is the L^2-projection onto $\underline{\boldsymbol{A}}_h^c$, and $C^c > 0$ is a constant independent of h.

Let us consider the orthogonal decomposition

$$\boldsymbol{\gamma}_h = \boldsymbol{\gamma}_h^0 + \boldsymbol{\gamma}_h^c \quad \text{where} \quad \boldsymbol{\gamma}_h^c|_K := \frac{1}{|K|}\int_K \boldsymbol{\gamma}_h, \forall K \in \mathcal{T}_E \quad \text{(component-wise)} \quad \text{and} \quad \boldsymbol{\gamma}_h^0 = \boldsymbol{\gamma}_h - \boldsymbol{\gamma}_h^c.$$

It is clear that $\boldsymbol{\gamma}_h^0 \in \underline{\boldsymbol{A}}_h^0$ and $\boldsymbol{\gamma}_h^c \in \underline{\boldsymbol{A}}_h^c$.

By [35, Lemma 3.9], there exists

$$\boldsymbol{v}^0 \in \underline{\boldsymbol{\mathcal{B}}_h} := \{\boldsymbol{\eta} \in \underline{\boldsymbol{L}}^2(\Omega_E) : \boldsymbol{\eta}|_K \in \underline{\boldsymbol{B}}(K)\,, K \in \mathcal{T}_E\} \subset \underline{\boldsymbol{V}}_h$$

such that

$$(\boldsymbol{\gamma}_h^0, \boldsymbol{\rho}^0)_{\mathcal{T}_E} = (\boldsymbol{v}^0, \boldsymbol{\rho}^0)_{\mathcal{T}_E} \quad \text{for all } \boldsymbol{\rho}^0 \in \underline{\boldsymbol{A}}_h. \tag{1.10}$$

Taking $\boldsymbol{\tau} = \boldsymbol{v}^0$ in (1.5a), we obtain

$$(\boldsymbol{\gamma}_h^0 + \boldsymbol{\gamma}_h^c, \boldsymbol{v}^0)_{\mathcal{T}_E} = 0.$$

Now, considering $\boldsymbol{\rho}^0 = \boldsymbol{\gamma}_h^c$, and the fact that the decomposition of $\boldsymbol{\gamma}_h$ is orthogonal in $\underline{\boldsymbol{L}}^2$, the two expressions above imply

$$(\boldsymbol{\gamma}_h^0, \boldsymbol{v}^0)_{\mathcal{T}_E} = (\boldsymbol{\gamma}_h^0, \boldsymbol{\gamma}_h^c)_{\mathcal{T}_E} = 0.$$

Hence, taking $\boldsymbol{\rho}^0 = \boldsymbol{\gamma}_h^0$ in (1.10), the equality above shows that $(\boldsymbol{\gamma}_h^0, \boldsymbol{v}^0)_{\mathcal{T}_E} = \|\boldsymbol{\gamma}_h^0\|^2_{\mathcal{T}_E} = 0$, and we can conclude that $\boldsymbol{\gamma}_h^0 = \boldsymbol{0}$.

Finally, by the second property in (1.9), there exists $\boldsymbol{v}^c \in \boldsymbol{H}(\mathrm{div};\Omega_E) \cap \underline{\boldsymbol{\mathcal{P}}}_1(\mathcal{T}_E)$ such that

$$(\boldsymbol{v}^c, \boldsymbol{\rho}^c)_{\mathcal{T}_E} = (\boldsymbol{\gamma}_h^c, \boldsymbol{\rho}^c)_{\mathcal{T}_E} \quad \text{for all } \boldsymbol{\rho}^c \in \underline{\boldsymbol{A}}_h^c.$$

Taking $\boldsymbol{\rho}^c = \boldsymbol{\gamma}_h^c$ in the expression above we have

$$(\boldsymbol{\gamma}_h^c, \boldsymbol{v}^c)_{\mathcal{T}_E} = \|\boldsymbol{\gamma}_h^c\|^2_{\mathcal{T}_E}\,. \tag{1.11}$$

Now, recalling that $\boldsymbol{\sigma}_h = \mathbf{0}$ and $\boldsymbol{u}_h = \mathbf{0}$ in $\mathcal{T}_E$ and $\widehat{\boldsymbol{u}}_h = \mathbf{0}$ on $\partial\mathcal{T}_E$, choosing $\boldsymbol{\tau} = \boldsymbol{v}^c$ in (1.5a), we have that $(\boldsymbol{\gamma}_h, \boldsymbol{v}^c)_{\mathcal{T}_E} = 0$. Then, since $\boldsymbol{\gamma}_h^0 = \mathbf{0}$, from (1.11) we conclude $\boldsymbol{\gamma}_h^c = \mathbf{0}$ in $\mathcal{T}_E$, and therefore $\boldsymbol{\gamma}_h = 0$. ■

1.4.2 Error Analysis.

1.4.2.1 The HDG Projections.

We will need the HDG projections defined in [21]. For the acoustic terms, the projected function is denoted by $\boldsymbol{\Pi_h^A}(\boldsymbol{q}, v) := \left(\boldsymbol{\Pi_W^A q}, \Pi_W v\right)$, where $\boldsymbol{\Pi_W^A q}$ and $\Pi_W v$ are the components of the projection in $\boldsymbol{W}_h^A$ and W_h, respectively. The values of the projection on any simplex $K \in \mathcal{T}_A$ are fixed when the components are required to satisfy the equations

$$
\begin{aligned}
\left(\boldsymbol{\Pi_W^A q}, \boldsymbol{r}\right)_K &= (\boldsymbol{q}, \boldsymbol{r})_K, && \forall \boldsymbol{r} \in \boldsymbol{\mathcal{P}}_{k-1}(K)\,, \\
(\Pi_W v, w)_K &= (v, w)_K, && \forall w \in \mathcal{P}_{k-1}(K)\,, \\
\left\langle \boldsymbol{\Pi_W^A q} \cdot \boldsymbol{n} - \tau_A \Pi_W v, \xi \right\rangle_F &= \langle \boldsymbol{q} \cdot \boldsymbol{n} - \tau_A P_M v, \xi \rangle_F\,, && \forall \xi \in \mathcal{P}_k(F)\,,
\end{aligned}
$$

for all faces F of the simplex $K \in \mathcal{T}_A$, where P_M is the L^2 projection onto F. It was shown in [21] that, if $(\boldsymbol{q}, v) \in \boldsymbol{H}^{k+1}(K) \times H^{k+1}(K)$ and $\tau_A|_{\partial K}$ is nonnegative and $\max\limits_{\partial K} \tau_A > 0$, the components of the projection satisfy the estimates

$$
\left\|\boldsymbol{\Pi_W^A q} - \boldsymbol{q}\right\|_K \lesssim h_K^{k+1} \left(|\boldsymbol{q}|_{\boldsymbol{H}^{k+1}(K)} + |v|_{H^{k+1}(K)}\right), \tag{1.12a}
$$

$$
\|\Pi_W v - v\|_K \lesssim h_K^{k+1} \left(|v|_{H^{k+1}(K)} + |\nabla \cdot \boldsymbol{q}|_{H^k(K)}\right). \tag{1.12b}
$$

Therefore, for the sake of simplicity, from now on we assume that τ_E and τ_A are positive functions.

For the elastic terms, on each element $K \in \mathcal{T}_E$, a component-wise version of the above projection is defined by $\boldsymbol{\Pi_h^E}(\boldsymbol{\sigma}, \boldsymbol{u}) := \left(\boldsymbol{\Pi_V \sigma}, \boldsymbol{\Pi_W^E u}\right) \in \underline{\boldsymbol{\mathcal{P}}}_k(K) \times \boldsymbol{\mathcal{P}}_k(K)$ where

$$
\begin{aligned}
\left(\boldsymbol{\Pi_V \sigma}, \boldsymbol{\tau}\right)_K &= (\boldsymbol{\sigma}, \boldsymbol{\tau})_K, && \forall \boldsymbol{\tau} \in \underline{\boldsymbol{\mathcal{P}}}_{k-1}(K)\,, \\
\left(\boldsymbol{\Pi_W^E u}, \boldsymbol{t}\right)_K &= (\boldsymbol{u}, \boldsymbol{t})_K, && \forall \boldsymbol{t} \in \boldsymbol{\mathcal{P}}_{k-1}(K)\,,
\end{aligned}
$$

$$\left\langle (\boldsymbol{\Pi_V}\boldsymbol{\sigma})\boldsymbol{n} - \tau_E \boldsymbol{\Pi}_{\boldsymbol{W}}^{\boldsymbol{E}}\boldsymbol{u}, \boldsymbol{\mu} \right\rangle_F = \langle \boldsymbol{\sigma}\boldsymbol{n} - \tau_E \boldsymbol{P_M}\boldsymbol{u}, \boldsymbol{\mu}\rangle_F , \qquad \forall \boldsymbol{\mu} \in \boldsymbol{\mathcal{P}}_k(F) ,$$

for all faces F of the element $K \in \mathcal{T}_E$. Above, $\boldsymbol{P_M}$ is the $\boldsymbol{L}^2$ projection onto F. Analogously, if $(\boldsymbol{\sigma}, \boldsymbol{u}) \in \underline{\boldsymbol{H}}^{k+1}(K) \times \boldsymbol{H}^{k+1}(K)$, then

$$\|\boldsymbol{\Pi_V}\boldsymbol{\sigma} - \boldsymbol{\sigma}\|_K \lesssim h_K^{k+1} \left(|\boldsymbol{\sigma}|_{\underline{\boldsymbol{H}}^{k+1}(K)} + |\boldsymbol{u}|_{\boldsymbol{H}^{k+1}(K)} \right), \tag{1.13a}$$

$$\left\|\boldsymbol{\Pi}_{\boldsymbol{W}}^{\boldsymbol{E}}\boldsymbol{u} - \boldsymbol{u}\right\|_K \lesssim h_K^{k+1} \left(|\boldsymbol{u}|_{\boldsymbol{H}^{k+1}(K)} + |\nabla\cdot\boldsymbol{\sigma}|_{\underline{\boldsymbol{H}}^{k}(K)} \right). \tag{1.13b}$$

In addition, for each element $K \in \mathcal{T}_E$, we will denote by $\boldsymbol{\Pi_A}\boldsymbol{\gamma}$ the $\underline{\boldsymbol{L}}^2(K)$-projection of $\boldsymbol{\gamma}$ on $\underline{\boldsymbol{A}}(K)$. Thus, if $\boldsymbol{\gamma} \in \underline{\boldsymbol{H}}^{k+1}(K)$, then

$$\|\boldsymbol{\Pi_A}\boldsymbol{\gamma} - \boldsymbol{\gamma}\|_K \lesssim h_K^{k+1} |\gamma|_{\underline{\boldsymbol{H}}^{k+1}(K)} .$$

Having defined the projections, we now define the *projection errors* in each of the volume unknowns by

$$\begin{aligned}
&\boldsymbol{\delta_\sigma} := \boldsymbol{\sigma} - \boldsymbol{\Pi_V}\boldsymbol{\sigma}, \qquad \boldsymbol{\delta_u} := \boldsymbol{u} - \boldsymbol{\Pi}_{\boldsymbol{W}}^{\boldsymbol{E}}\boldsymbol{u}, \qquad \boldsymbol{\delta_\gamma} := \boldsymbol{\gamma} - \boldsymbol{\Pi_A}\boldsymbol{\gamma},\\
&\boldsymbol{\delta_q} := \boldsymbol{q} - \boldsymbol{\Pi}_{\boldsymbol{W}}^{\boldsymbol{A}}\boldsymbol{q}, \qquad \delta_v := v - \Pi_W v.
\end{aligned}$$

The following quantity will play a fundamental role in the error estimations:

$$\Theta(\boldsymbol{\sigma}, \boldsymbol{u}, \boldsymbol{\gamma}, \boldsymbol{q}, v) := \left(\|\boldsymbol{\delta_\sigma}\|^2_{\mathcal{T}_E} + \|\boldsymbol{\delta_u}\|^2_{\mathcal{T}_E} + \|\boldsymbol{\delta_\gamma}\|^2_{\mathcal{T}_E} + \|\boldsymbol{\delta_q}\|^2_{\mathcal{T}_A} + \|\delta_v\|^2_{\mathcal{T}_A} \right)^{1/2} .$$

The next lemma follows readily from the projection bounds (1.12) and (1.13).

Lemma 2. *If* $(\boldsymbol{\sigma}, \boldsymbol{u}, \boldsymbol{\gamma}, \boldsymbol{q}, v) \in \underline{\boldsymbol{H}}^{k+1}(\Omega_E) \times \boldsymbol{H}^{k+1}(\Omega_E) \times \underline{\boldsymbol{H}}^{k+1}(\Omega_E) \times \boldsymbol{H}^{k+1}(\Omega_A) \times H^{k+1}(\Omega_A)$, *then*

$$\Theta(\boldsymbol{\sigma}, \boldsymbol{u}, \boldsymbol{\gamma}, \boldsymbol{q}, v) \lesssim \;\; h^{k+1} \left(|\boldsymbol{\sigma}|_{\underline{\boldsymbol{H}}^{k+1}(\Omega_E)} + |\boldsymbol{u}|_{\boldsymbol{H}^{k+1}(\Omega_E)} + |\boldsymbol{\gamma}|_{\underline{\boldsymbol{H}}^{k+1}(\Omega_E)} + |\boldsymbol{q}|_{\boldsymbol{H}^{k+1}(\Omega_A)} + |v|_{H^{k+1}(\Omega_A)} \right).$$

1.4.2.2 Error estimates.

Let us define the *projections of the errors* (not to be confused with the projection errors defined above):

$$\boldsymbol{e_\sigma} := \boldsymbol{\Pi_V}\boldsymbol{\sigma} - \boldsymbol{\sigma}_h, \qquad \boldsymbol{e}_{\widehat{\boldsymbol{\sigma}}}\boldsymbol{n} := \boldsymbol{P_M}(\boldsymbol{\sigma}\boldsymbol{n}) - \widehat{\boldsymbol{\sigma}}_h\boldsymbol{n}, \qquad \boldsymbol{e_u} := \boldsymbol{\Pi}_{\boldsymbol{W}}^{\boldsymbol{E}}\boldsymbol{u} - \boldsymbol{u}_h,$$

$$e_{\widehat{\boldsymbol{u}}} := \boldsymbol{P_M u} - \widehat{\boldsymbol{u}}_h, \qquad \boldsymbol{e_\gamma} := \boldsymbol{\Pi_A \gamma} - \boldsymbol{\gamma}_h, \qquad \boldsymbol{e_q} := \boldsymbol{\Pi_W^A q} - \boldsymbol{q}_h,$$

$$\boldsymbol{e}_{\widehat{\boldsymbol{q}}}\cdot\boldsymbol{n} := P_M(\boldsymbol{q}\cdot\boldsymbol{n}) - \boldsymbol{q}_h\cdot\boldsymbol{n}, \qquad e_v := \Pi_W v - v_h, \qquad e_{\widehat{v}} := P_M v - \widehat{v}_h.$$

Direct calculations imply that, for all $(\boldsymbol{\tau}, \boldsymbol{t}, \boldsymbol{\eta}, \boldsymbol{\mu}, \boldsymbol{r}, w, \xi) \in \underline{\boldsymbol{V}}_h \times \boldsymbol{W}_h^E \times \underline{\boldsymbol{A}}_h \times \boldsymbol{M}_h \times \boldsymbol{W}_h^A \times W_h \times M_h$, the projections of the errors satisfy the following system:

$$(\mathbf{C}^{-1}\boldsymbol{e_\sigma}, \boldsymbol{\tau})_{\mathcal{T}_E} + (\boldsymbol{e_u}, \nabla\cdot\boldsymbol{\tau})_{\mathcal{T}_E} + (\boldsymbol{e_\gamma}, \boldsymbol{\tau})_{\mathcal{T}_E} - \langle \boldsymbol{e}_{\widehat{\boldsymbol{u}}}, \boldsymbol{\tau n}\rangle_{\partial\mathcal{T}_E} = -(\mathbf{C}^{-1}\boldsymbol{\delta_\sigma}, \boldsymbol{\tau})_{\mathcal{T}_E} - (\boldsymbol{\delta_\gamma}, \boldsymbol{\tau})_{\mathcal{T}_E}, \tag{1.14a}$$

$$(\boldsymbol{e_\sigma}, \nabla \boldsymbol{t})_{\mathcal{T}_E} - \langle \boldsymbol{e}_{\widehat{\boldsymbol{\sigma}}}\boldsymbol{n}, \boldsymbol{t}\rangle_{\partial\mathcal{T}_E} + \rho_E s^2(\boldsymbol{e_u}, \boldsymbol{t})_{\mathcal{T}_E} = -\rho_E s^2(\boldsymbol{\delta_u}, \boldsymbol{t})_{\mathcal{T}_E}, \tag{1.14b}$$

$$(\boldsymbol{e_\sigma}, \boldsymbol{\eta})_{\mathcal{T}_E} = -(\boldsymbol{\delta_\sigma}, \boldsymbol{\eta})_{\mathcal{T}_E}, \tag{1.14c}$$

$$\langle \boldsymbol{e}_{\widehat{\boldsymbol{\sigma}}}\boldsymbol{n}, \boldsymbol{\mu}\rangle_{\partial\mathcal{T}_E\setminus\Gamma} = 0, \tag{1.14d}$$

$$(\boldsymbol{e_q}, \boldsymbol{r})_{\mathcal{T}_A} + (e_v, \nabla\cdot\boldsymbol{r})_{\mathcal{T}_A} - \langle e_{\widehat{v}}, \boldsymbol{r}\cdot\boldsymbol{n}\rangle_{\partial\mathcal{T}_A} = -(\boldsymbol{\delta_q}, \boldsymbol{r})_{\mathcal{T}_A}, \tag{1.14e}$$

$$(\boldsymbol{e_q}, \nabla w)_{\mathcal{T}_A} - \langle \boldsymbol{e}_{\widehat{\boldsymbol{q}}}\cdot\boldsymbol{n}, w\rangle_{\partial\mathcal{T}_A} + (s/c)^2(e_v, w)_{\mathcal{T}_A} = -(s/c)^2(\delta_v, w)_{\mathcal{T}_A}, \tag{1.14f}$$

$$\langle \boldsymbol{e}_{\widehat{\boldsymbol{q}}}\cdot\boldsymbol{n}, \xi\rangle_{\partial\mathcal{T}_A\setminus(\Gamma\cup\Gamma_A^D)} = 0, \tag{1.14g}$$

$$\langle e_{\widehat{v}}, \xi\rangle_{\Gamma_A^D} = 0, \tag{1.14h}$$

$$\langle \boldsymbol{e}_{\widehat{\boldsymbol{q}}}\cdot\boldsymbol{n}_A - s\,\boldsymbol{e}_{\widehat{\boldsymbol{u}}}\cdot\boldsymbol{n}_E, \xi\rangle_\Gamma = 0, \tag{1.14i}$$

$$\langle -\boldsymbol{e}_{\widehat{\boldsymbol{\sigma}}}\boldsymbol{n}_E + \rho_f s\, e_{\widehat{v}}\,\boldsymbol{n}_A, \boldsymbol{\mu}\rangle_\Gamma = 0 \tag{1.14j}$$

while $\boldsymbol{e}_{\widehat{\boldsymbol{\sigma}}}$ and $\boldsymbol{e}_{\widehat{\boldsymbol{q}}}$ satisfy

$$\boldsymbol{e}_{\widehat{\boldsymbol{\sigma}}}\boldsymbol{n} = \boldsymbol{e_\sigma n} - \tau_E(\boldsymbol{e_u} - \boldsymbol{e}_{\widehat{\boldsymbol{u}}}) \quad \text{on } \partial\mathcal{T}_E,$$

$$\boldsymbol{e}_{\widehat{\boldsymbol{q}}}\cdot\boldsymbol{n} = \boldsymbol{e_q}\cdot\boldsymbol{n} - \tau_A(e_v - e_{\widehat{v}}) \quad \text{on } \partial\mathcal{T}_A.$$

The following lemma can be proven by arguing as in the first part of the proof of Theorem 1.

Lemma 3. *The projections of the errors satisfy*

$$e_E^2 + e_A^2 + \rho_E|s|^2\mathrm{Re}(s)\,\|\boldsymbol{e_u}\|_{\mathcal{T}_E}^2 + \frac{\rho_f}{c^2}|s|^2\mathrm{Re}(s)\,\|e_v\|_{\mathcal{T}_A}^2$$

$$
\begin{aligned}
&= -\operatorname{Re}\big(s(\mathbf{C}^{-1}\boldsymbol{\delta}_{\boldsymbol{\sigma}}, \boldsymbol{e}_{\boldsymbol{\sigma}})_{\mathcal{T}_E}\big) + \operatorname{Re}(s(\boldsymbol{e}_{\boldsymbol{\gamma}}, \boldsymbol{\delta}_{\boldsymbol{\sigma}})_{\mathcal{T}_E}) - \operatorname{Re}(s(\boldsymbol{\delta}_{\boldsymbol{\gamma}}, \boldsymbol{e}_{\boldsymbol{\sigma}})_{\mathcal{T}_E}) \\
&\quad - \rho_E |s|^2 \operatorname{Re}(s(\boldsymbol{e}_{\boldsymbol{u}}, \boldsymbol{\delta}_{\boldsymbol{u}})_{\mathcal{T}_E}) - \rho_f \operatorname{Re}(\overline{s}(\boldsymbol{e}_{\boldsymbol{q}}, \boldsymbol{\delta}_{\boldsymbol{q}})_{\mathcal{T}_A}) - \frac{\rho_f}{c^2}|s|^2 \operatorname{Re}(s(\delta_v, e_v)_{\mathcal{T}_A}),
\end{aligned}
\tag{1.15}
$$

where

$$
e_E := \sqrt{\left\| \operatorname{Re}(s)^{1/2}\, \boldsymbol{e}_{\boldsymbol{\sigma}} \right\|^2_{\mathcal{T}_E, \mathbf{C}^{-1}} + \left\| \operatorname{Re}(s)^{1/2}\, \tau_E^{1/2} (\boldsymbol{e}_{\boldsymbol{u}} - \boldsymbol{e}_{\widehat{\boldsymbol{u}}}) \right\|^2_{\partial \mathcal{T}_E}},
$$

$$
e_A := \sqrt{\left\| \rho_f^{1/2} \operatorname{Re}(s)^{1/2}\, \boldsymbol{e}_{\boldsymbol{q}} \right\|^2_{\mathcal{T}_A} + \left\| \rho_f^{1/2} \operatorname{Re}(s)^{1/2}\, \tau_A^{1/2} (e_v - e_{\widehat{v}}) \right\|^2_{\partial \mathcal{T}_A}}.
$$

Applying the triangle, Cauchy-Schwarz and Young inequalities several times to the expression (1.15), we can obtain the key inequality:

$$
e_E^2 + e_A^2 + \rho_E |s|^2 \operatorname{Re}(s) \left\| \boldsymbol{e}_{\boldsymbol{u}} \right\|^2_{\mathcal{T}_E} + \frac{\rho_f}{c^2}|s|^2 \operatorname{Re}(s) \left\| e_v \right\|^2_{\mathcal{T}_A} \lesssim \Theta(\boldsymbol{\sigma}, \boldsymbol{u}, \boldsymbol{\gamma}, \boldsymbol{q}, v). \tag{1.16}
$$

Using this result, it is possible to obtain bounds for the error in each unknown:

Theorem 4. *If* $(\boldsymbol{\sigma}, \boldsymbol{u}, \boldsymbol{\gamma}, \boldsymbol{q}, v) \in \underline{\boldsymbol{H}}^{k+1}(\Omega_E) \times \boldsymbol{H}^{k+1}(\Omega_E) \times \underline{\boldsymbol{H}}^{k+1}(\Omega_E) \times \boldsymbol{H}^{k+1}(\Omega_A) \times H^{k+1}(\Omega_A)$, *then*

$$
||\boldsymbol{\sigma} - \boldsymbol{\sigma}_h||_{\mathcal{T}_E} + ||\boldsymbol{u} - \boldsymbol{u}_h||_{\mathcal{T}_E} + ||\boldsymbol{\gamma} - \boldsymbol{\gamma}_h||_{\mathcal{T}_E} + ||\boldsymbol{q} - \boldsymbol{q}_h||_{\mathcal{T}_A} + ||v - v_h||_{\mathcal{T}_A} \lesssim \Theta(\boldsymbol{\sigma}, \boldsymbol{u}, \boldsymbol{\gamma}, \boldsymbol{q}, v).
$$

Proof. Let us explain the bound for the norm of the error in $\boldsymbol{\sigma}$. Have in mind that $\boldsymbol{\sigma} - \boldsymbol{\sigma}_h = \boldsymbol{e}_{\boldsymbol{\sigma}} + \boldsymbol{\delta}_{\boldsymbol{\sigma}}$, so

$$
\begin{aligned}
||\boldsymbol{\sigma} - \boldsymbol{\sigma}_h||^2_{\mathcal{T}_E} &= ||\boldsymbol{e}_{\boldsymbol{\sigma}} + \boldsymbol{\delta}_{\boldsymbol{\sigma}}||^2_{\mathcal{T}_E} \lesssim ||\boldsymbol{e}_{\boldsymbol{\sigma}}||^2_{\mathcal{T}_E} + ||\boldsymbol{\delta}_{\boldsymbol{\sigma}}||^2_{\mathcal{T}_E} \\
&\lesssim 2\mu \left\| \boldsymbol{e}_{\boldsymbol{\sigma}} \right\|^2_{\mathcal{T}_E, \mathbf{C}^{-1}} + \Theta^2(\boldsymbol{\sigma}, \boldsymbol{u}, \boldsymbol{\gamma}, \boldsymbol{q}, v) \lesssim \Theta^2(\boldsymbol{\sigma}, \boldsymbol{u}, \boldsymbol{\gamma}, \boldsymbol{q}, v).
\end{aligned}
$$

Where we use the relation between the norms $\|\cdot\|_{\mathcal{T}_E}$ and $\|\cdot\|_{\mathcal{T}_E, \mathbf{C}^{-1}}$ and (1.16). In the case of the other unknowns, the procedure is similar. ∎

1.5 Numerical Experiments

On the set of the element boundaries, for $\dagger \in \{A, E\}$, we consider the norm

$$
|||\cdot|||_{\partial \mathcal{T}_\dagger} := \left(\sum_{K \in \mathcal{T}_\dagger} h_K \| \cdot \|^2_{\partial K} \right)^{1/2}.
$$

Given an unknown ϕ and two approximations ϕ_h and $\phi_{\tilde{h}}$ associated to two consecutive meshes of sizes h and $\tilde{h}$, we compute the experimental order of convergence (e.o.c.) of the error in ϕ in the $\|\|$-norm as $\log\left(\|\phi-\phi_h\|/\|\phi-\phi_{\tilde{h}}\|\right)/\log\left(h/\tilde{h}\right)$.

1.5.1 Acoustics problem.

To test our HDG scheme applied to the acoustics problem, we consider equations (1.1c)-(1.1d) complemented with Dirichlet boundary conditions $v = g_D$ on $\partial\Omega_A$. We take a manufactured acoustic field $v(x, y) = \sin(x)\sin(y)$. The source f and boundary data g_D are set in such a way that v satisfies (1.1c)-(1.1d) in a domain $\Omega_A = (0, 1)^2$, with $c = 1$ and, for example, $s = 2 - i$.

The stabilization parameter τ_A is taken to be equal to one everywhere. We consider quasi-uniform refinements of Ω_A and set $k \in \{1, 2, 3\}$ in the local spaces.

The Table 1.1 shows the results obtained for this problem, where N is the number of mesh triangles. Note that for the errors in $\boldsymbol{q}$ and v the optimal theoretical order of convergence $k+1$ was reached. In turn, for the numerical trace we can see an order of superconvergence $k+2$. The Figure 1.2 graphically presents the data of this table.

k	N	$\|\boldsymbol{q}-\boldsymbol{q}_h\|_{\mathcal{T}_A}$	e.o.c.	$\|v-v_h\|_{\mathcal{T}_A}$	e.o.c.	$\|\|v-\widehat{v}_h\|\|_{\partial\mathcal{T}_A}$	e.o.c.
1	4	1.86e−02	–	9.65e−03	–	5.91e−03	–
	16	5.16e−03	1.85	2.48e−03	1.96	7.99e−04	2.89
	64	1.34e−03	1.95	6.40e−04	1.95	1.03e−04	2.95
	512	1.45e−04	2.14	5.96e−05	2.28	5.02e−06	2.91
	2048	3.62e−05	2.00	1.53e−05	1.96	6.29e−07	3.00
	8192	9.04e−06	2.00	3.89e−06	1.98	7.87e−08	3.00
2	4	1.74e−03	–	7.71e−04	–	4.09e−04	–
	16	1.94e−04	3.16	6.76e−05	3.51	2.64e−05	3.95
	64	2.33e−05	3.06	6.12e−06	3.46	1.69e−06	3.96
	512	3.56e−07	4.02	4.33e−07	2.55	2.87e−08	3.92
	2048	4.38e−08	3.02	5.06e−08	3.10	1.79e−09	4.00
	8192	5.43e−09	3.01	6.10e−09	3.05	1.12e−10	4.00
3	4	2.64e−05	–	7.23e−05	–	1.92e−05	–
	16	2.48e−06	3.41	4.44e−06	4.03	6.57e−07	4.87
	64	1.63e−07	3.93	2.72e−07	4.03	2.12e−08	4.96
	512	3.75e−09	3.63	9.72e−09	3.21	1.66e−10	4.66
	2048	2.42e−10	3.95	6.06e−10	4.00	5.19e−12	5.00
	8192	1.54e−11	3.98	3.78e−11	4.00	2.61e−13	4.31

Table 1.1: Results for the acoustics problem.

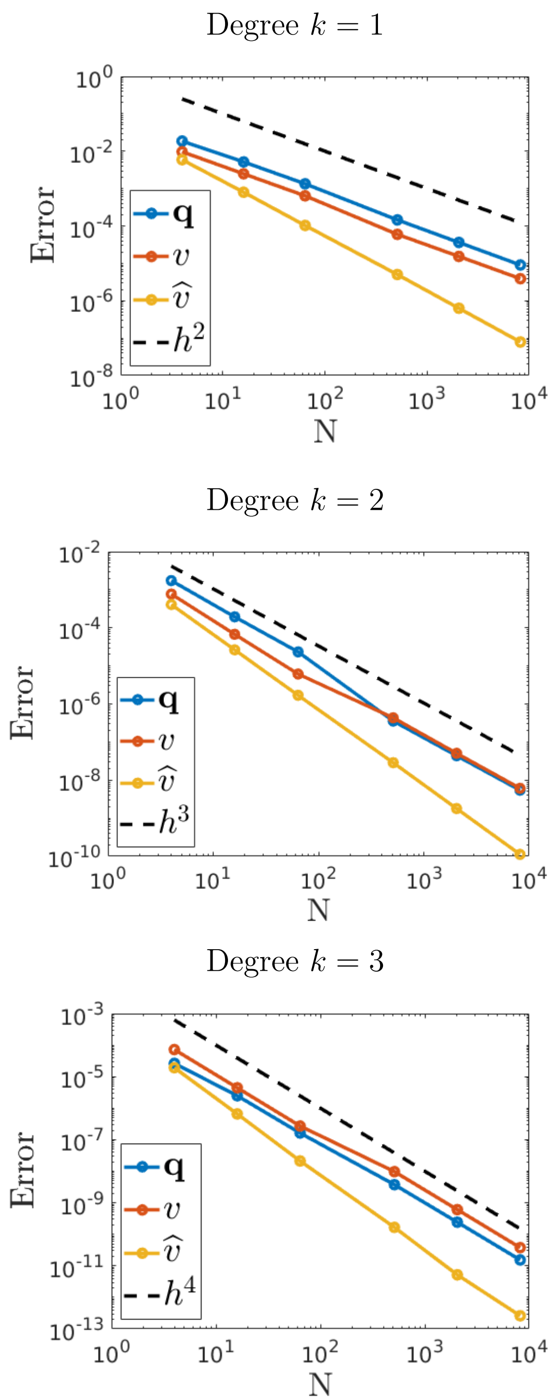

Figure 1.2: Discretization error as a function of the number of triangles in the domain for the acoustic problem.

1.5.2 Elastic problem.

Analogously to the previous subsection, let us apply the HDG scheme to the equations (1.3a)-(1.1b) considering $\Omega_E = (0,1)^2, \rho_E = 1, s = 2 - i$ and $\tau_E = 1$ everywhere. The source $\boldsymbol{f}$ and the Dirichlet boundary condition are defined such that

$$\boldsymbol{u}(x,y) = \begin{pmatrix} \sin(\pi x)\cos(\pi y) \\ \cos(\pi x)\sin(\pi y) \end{pmatrix}, \quad (x,y) \in (0,1)^2,$$

is the exact solution of the problem.

It is known that the Lamé's first parameter (λ) and the shear modulus (μ) (or Lamé's second parameter) satisfy the following expressions in terms of the Young's modulus (E) and the Poisson's ratio (ν):

$$\lambda = \frac{E\nu}{(1+\nu)(1-2\nu)} \qquad \text{and} \qquad \mu = \frac{E}{2(1+\nu)},$$

so let us take $E = 1$ and two values of ν: 0.3 and 0.49999 (a perfectly incompressible isotropic material deformed elastically at small strains would have a Poisson's ratio of exactly 0.5).

The numerical results are shown in Table 1.2 and Table 1.3. The same information is plotted in Figure 1.3. Observe that the experimental orders of convergence of the errors in $\boldsymbol{\sigma}, \boldsymbol{u}$ and $\boldsymbol{\gamma}$, $k+1$, coincide with the theoretical results. In addition, for the numerical trace of $\boldsymbol{u}$ we also have a superconvergence of order $k+2$.

k	N	$\|\boldsymbol{\sigma}-\boldsymbol{\sigma}_h\|_{\mathcal{T}_E}$	e.o.c.	$\|\boldsymbol{u}-\boldsymbol{u}_h\|_{\mathcal{T}_E}$	e.o.c.	$\|\!\|\boldsymbol{u}-\widehat{\boldsymbol{u}}_h\|\!\|_{\partial\mathcal{T}_E}$	e.o.c.	$\|\boldsymbol{\gamma}-\boldsymbol{\gamma}_h\|_{\mathcal{T}_E}$	e.o.c.
1	12	1.10e+00	–	5.71e−01	–	2.98e−01	–	2.92e−01	–
	48	6.81e−01	0.70	2.85e−01	1.01	8.67e−02	1.78	3.14e−01	−0.10
	192	1.80e−01	1.92	7.77e−02	1.87	1.43e−02	2.60	9.08e−02	1.79
	1536	2.08e−02	2.07	1.00e−02	1.97	5.86e−04	3.07	8.78e−03	2.25
	6144	5.22e−03	2.00	2.53e−03	1.98	7.54e−05	2.96	2.09e−03	2.07
	24576	1.31e−03	2.00	6.36e−04	1.99	9.53e−06	2.98	5.06e−04	2.05
2	12	9.76e−01	–	3.45e−01	–	1.75e−01	–	5.57e−01	–
	48	9.02e−02	3.44	3.79e−02	3.19	8.23e−03	4.41	4.22e−02	3.72
	192	1.16e−02	2.96	5.02e−03	2.92	5.25e−04	3.97	5.47e−03	2.95
	1536	5.43e−04	2.94	2.57e−04	2.86	8.07e−06	4.02	2.49e−04	2.97
	6144	6.80e−05	3.00	3.24e−05	2.99	4.97e−07	4.02	3.12e−05	3.00
	24576	8.51e−06	3.00	4.07e−06	2.99	3.09e−08	4.01	3.91e−06	3.00
3	12	4.64e−02	–	2.53e−02	–	8.33e−03	–	1.59e−02	–
	48	8.76e−03	2.41	3.77e−03	2.74	6.40e−04	3.70	4.70e−03	1.76
	192	5.63e−04	3.96	2.47e−04	3.94	2.29e−05	4.81	3.23e−04	3.86
	1536	1.21e−05	3.70	5.39e−06	3.68	2.02e−07	4.55	8.15e−06	3.54
	6144	7.58e−07	3.99	3.39e−07	3.99	6.54e−09	4.95	5.22e−07	3.96
	24576	4.74e−08	4.00	2.13e−08	4.00	2.07e−10	4.98	3.29e−08	3.99

Table 1.2: Results for the elastic problem, $\nu = 0.3$.

k	N	$\|\boldsymbol{\sigma}-\boldsymbol{\sigma}_h\|_{\mathcal{T}_E}$	e.o.c.	$\|\boldsymbol{u}-\boldsymbol{u}_h\|_{\mathcal{T}_E}$	e.o.c.	$\|\!\|\boldsymbol{u}-\widehat{\boldsymbol{u}}_h\|\!\|_{\partial\mathcal{T}_E}$	e.o.c.	$\|\boldsymbol{\gamma}-\boldsymbol{\gamma}_h\|_{\mathcal{T}_E}$	e.o.c.
1	12	1.41e+04	–	5.13e+03	–	2.22e+03	–	2.27e+03	–
	48	1.03e+04	0.46	3.48e+03	0.56	1.39e+03	0.67	3.90e+03	−0.78
	192	2.70e+03	1.93	9.39e+02	1.89	2.31e+02	2.59	1.18e+03	1.73
	1536	4.26e+02	1.78	1.19e+02	1.99	1.70e+01	2.51	3.57e+02	1.15
	6144	1.08e+02	1.98	2.99e+01	1.99	2.24e+00	2.92	9.36e+01	1.93
	24576	2.73e+01	1.99	7.51e+00	1.99	2.87e−01	2.97	2.38e+01	1.97
2	12	1.61e+04	–	4.53e+03	–	2.83e+03	–	7.32e+03	–
	48	1.34e+03	3.58	4.60e+02	3.30	1.36e+02	4.38	5.25e+02	3.80
	192	1.67e+02	3.00	6.03e+01	2.93	8.14e+00	4.06	4.53e+01	3.53
	1536	1.10e+01	2.62	3.03e+00	2.88	2.09e−01	3.52	6.70e+00	1.84
	6144	1.38e+00	2.99	3.81e−01	2.99	1.29e−02	4.02	8.49e−01	2.98
	24576	1.73e−01	3.00	4.77e−02	3.00	8.05e−04	4.00	1.07e−01	2.99
3	12	4.12e+02	–	1.62e+02	–	5.97e+01	–	1.50e+02	–
	48	1.31e+02	1.66	4.54e+01	1.83	1.05e+01	2.51	5.20e+01	1.53
	192	8.45e+00	3.95	2.95e+00	3.94	3.98e−01	4.72	3.71e+00	3.81
	1536	2.58e−01	3.36	6.32e−02	3.70	5.67e−03	4.09	2.24e−01	2.70
	6144	1.63e−02	3.99	3.97e−03	3.99	1.83e−04	4.95	1.45e−02	3.96
	24576	1.02e−03	3.99	2.48e−04	4.00	5.79e−06	4.98	9.15e−04	3.98

Table 1.3: Results for the elastic problem, $\nu = 0.49999$.

$\nu = 0.3$	$\nu = 0.49999$

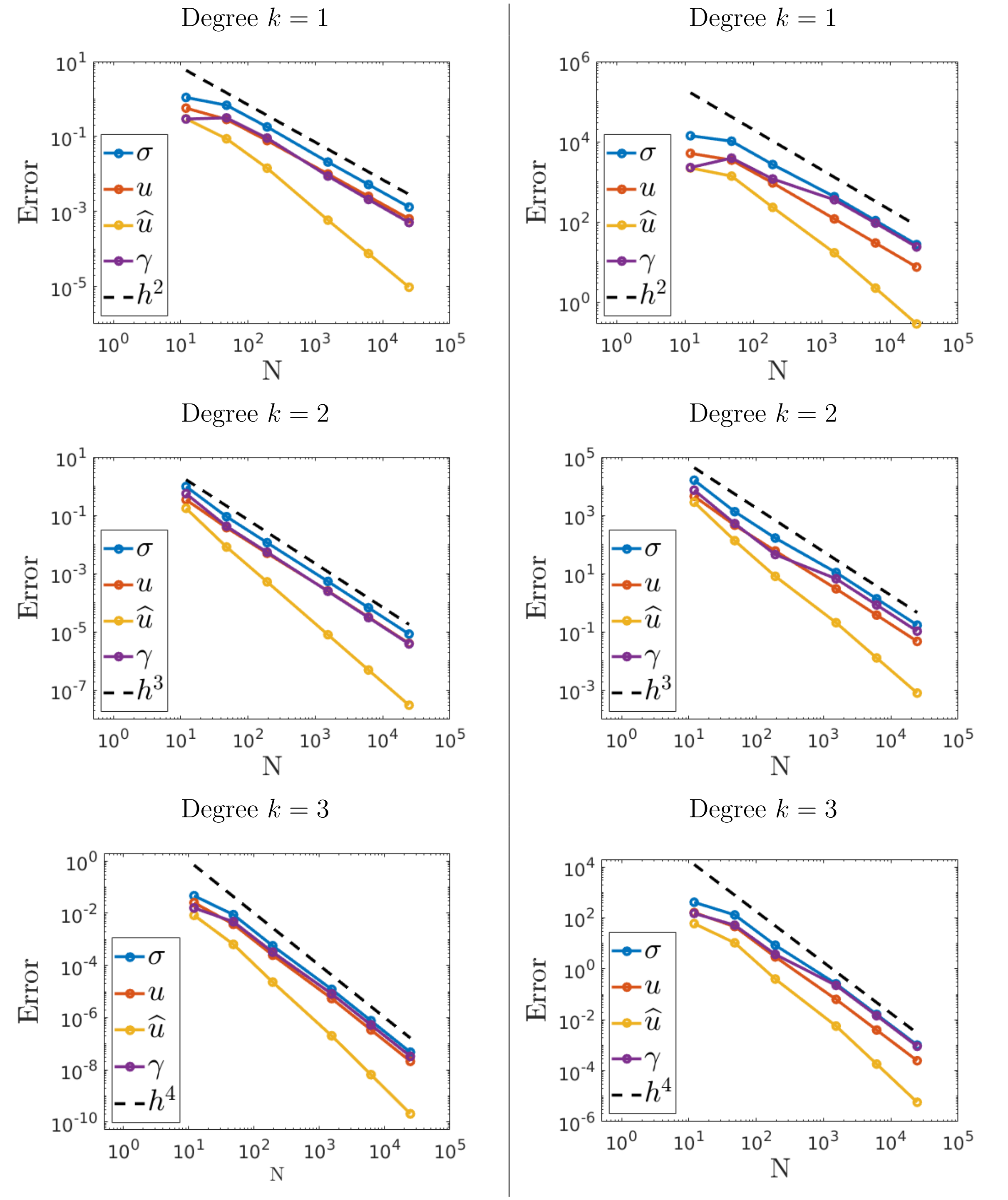

Figure 1.3: Discretization error as a function of the number of elements in the domain for Poisson's ratio $\nu = 0.3$ (first column) and $\nu = 0.49999$ (second column).

1.5.3 Coupled problem.

We now test our HDG scheme applied to the coupled problem (1.1a)-(1.1h) with Dirichlet boundary conditions $v = g_D$ on Γ_A. We take a manufactured acoustic field $v(x, y) = \sin(x)\sin(y)$. The source f and boundary data g_D are set in such a way that v satisfies (1.1c)-(1.1d) in a domain $\Omega_A = (-2, 2)^2$, with $c = 1$ and $s = 2 - i$. For the elastic region, we consider $\Omega_E = (-1, 1)^2, \rho_E = 1$ and $\tau_E = 1$ everywhere. The source $\boldsymbol{f}$ is defined such that

$$\boldsymbol{u}(x, y) = \begin{pmatrix} \sin(\pi x)\cos(\pi y) \\ \cos(\pi x)\sin(\pi y) \end{pmatrix}, \quad (x, y) \in (-1, 1)^2,$$

satisfies (1.1a)-(1.1b). We set the field $v^{\text{inc}}(x, y) = -\sin(x)\sin(y)$ and include additional terms on the right-hand sides of (1.1e)-(1.1f) so that our manufactured solution satisfies them.

In Table 1.4 and Table 1.5 we present the numerical results obtained. As in the acoustic and elastic problems, the experimental orders of convergence of $\boldsymbol{\sigma}$, $\boldsymbol{\gamma}$, $\boldsymbol{u}$, $\boldsymbol{q}$ and v coincide with the theoretical results. We also computationally obtain the superconvergence of order $k + 2$ for the numerical traces. In Figure 1.4 we graphically show the same results as in the tables.

k	N_e	$\|\boldsymbol{\sigma}-\boldsymbol{\sigma}_h\|_{\mathcal{T}_E}$	e.o.c.	$\|\boldsymbol{u}-\boldsymbol{u}_h\|_{\mathcal{T}_E}$	e.o.c.	$\|\|\boldsymbol{u}-\widehat{\boldsymbol{u}}_h\|\|_{\partial\mathcal{T}_E}$	e.o.c.	$\|\boldsymbol{\gamma}-\boldsymbol{\gamma}_h\|_{\mathcal{T}_E}$	e.o.c.
1	80	1.50e+00	–	8.98e−01	–	7.30e−01	–	6.07e−01	–
	306	4.84e−01	1.54	2.56e−01	1.71	8.22e−02	2.98	1.99e−01	1.52
	1210	1.33e−01	1.92	6.57e−02	2.02	1.04e−02	3.08	6.65e−02	1.63
	4824	3.25e−02	2.03	1.62e−02	2.02	1.18e−03	3.13	1.54e−02	2.11
	19202	8.26e−03	1.99	4.06e−03	2.00	1.50e−04	2.99	3.87e−03	2.00
	76638	2.10e−03	1.97	1.02e−03	1.99	1.93e−05	2.96	9.98e−04	1.96
2	80	5.13e−01	–	2.48e−01	–	1.11e−01	–	2.31e−01	–
	306	6.67e−02	2.78	2.82e−02	2.97	6.73e−03	3.82	3.07e−02	2.75
	1210	7.50e−03	3.24	3.77e−03	2.99	3.25e−04	4.50	3.38e−03	3.28
	4824	9.28e−04	3.01	4.55e−04	3.05	1.85e−05	4.12	3.85e−04	3.13
	19202	1.17e−04	3.00	5.76e−05	3.00	1.13e−06	4.05	4.78e−05	3.03
	76638	1.52e−05	2.95	7.28e−06	2.99	7.56e−08	3.91	6.25e−06	2.93
3	80	6.77e−02	–	3.43e−02	–	1.07e−02	–	3.76e−02	–
	306	6.22e−03	3.26	2.78e−03	3.43	4.54e−04	4.31	2.83e−03	3.53
	1210	3.75e−04	4.17	1.72e−04	4.13	1.35e−05	5.22	1.87e−04	4.03
	4824	2.18e−05	4.10	1.02e−05	4.06	3.57e−07	5.23	9.96e−06	4.23
	19202	1.44e−06	3.94	6.59e−07	3.98	1.21e−08	4.90	6.38e−07	3.99
	76638	9.50e−08	3.93	4.27e−08	3.95	4.05e−10	4.90	4.15e−08	3.94

Table 1.4: History of convergence of the coupled problem. Elastic region with a mesh of N_e elements.

k	N_a	$\|\boldsymbol{q}-\boldsymbol{q}_h\|_{\mathcal{T}_A}$	e.o.c.	$\|v-v_h\|_{\mathcal{T}_A}$	e.o.c.	$\|\|v-\widehat{v}_h\|\|_{\partial\mathcal{T}_A}$	e.o.c.
1	80	1.60e−01	–	2.41e−02	–	1.40e−01	–
	306	2.10e−02	3.02	4.98e−03	2.35	1.39e−02	3.44
	1210	3.69e−03	2.53	9.86e−04	2.36	1.88e−03	2.90
	4824	8.40e−04	2.14	2.30e−04	2.10	2.16e−04	3.13
	19202	2.05e−04	2.04	6.04e−05	1.94	2.83e−05	2.94
	76638	5.17e−05	1.99	1.51e−05	2.00	3.47e−06	3.03
2	80	3.25e−02	–	6.63e−03	–	2.96e−02	–
	306	1.81e−03	4.31	2.32e−04	5.00	7.76e−04	5.43
	1210	6.41e−05	4.86	1.19e−05	4.33	2.52e−05	4.99
	4824	4.11e−06	3.97	1.88e−06	2.66	5.67e−07	5.49
	19202	5.48e−07	2.92	2.54e−07	2.90	1.97e−08	4.86
	76638	6.66e−08	3.05	3.00e−08	3.09	8.18e−10	4.60
3	80	1.82e−03	–	2.45e−04	–	1.36e−03	–
	306	1.05e−04	4.26	1.13e−05	4.59	2.35e−05	6.05
	1210	2.35e−06	5.53	6.27e−07	4.21	1.96e−07	6.97
	4824	4.69e−08	5.66	4.48e−08	3.81	1.61e−09	6.94
	19202	2.64e−09	4.17	2.71e−09	4.06	3.55e−11	5.52
	76638	1.46e−10	4.18	1.77e−10	3.94	1.77e−12	4.33

Table 1.5: History of convergence of the coupled problem. Acoustic region with a mesh of N_a elements.

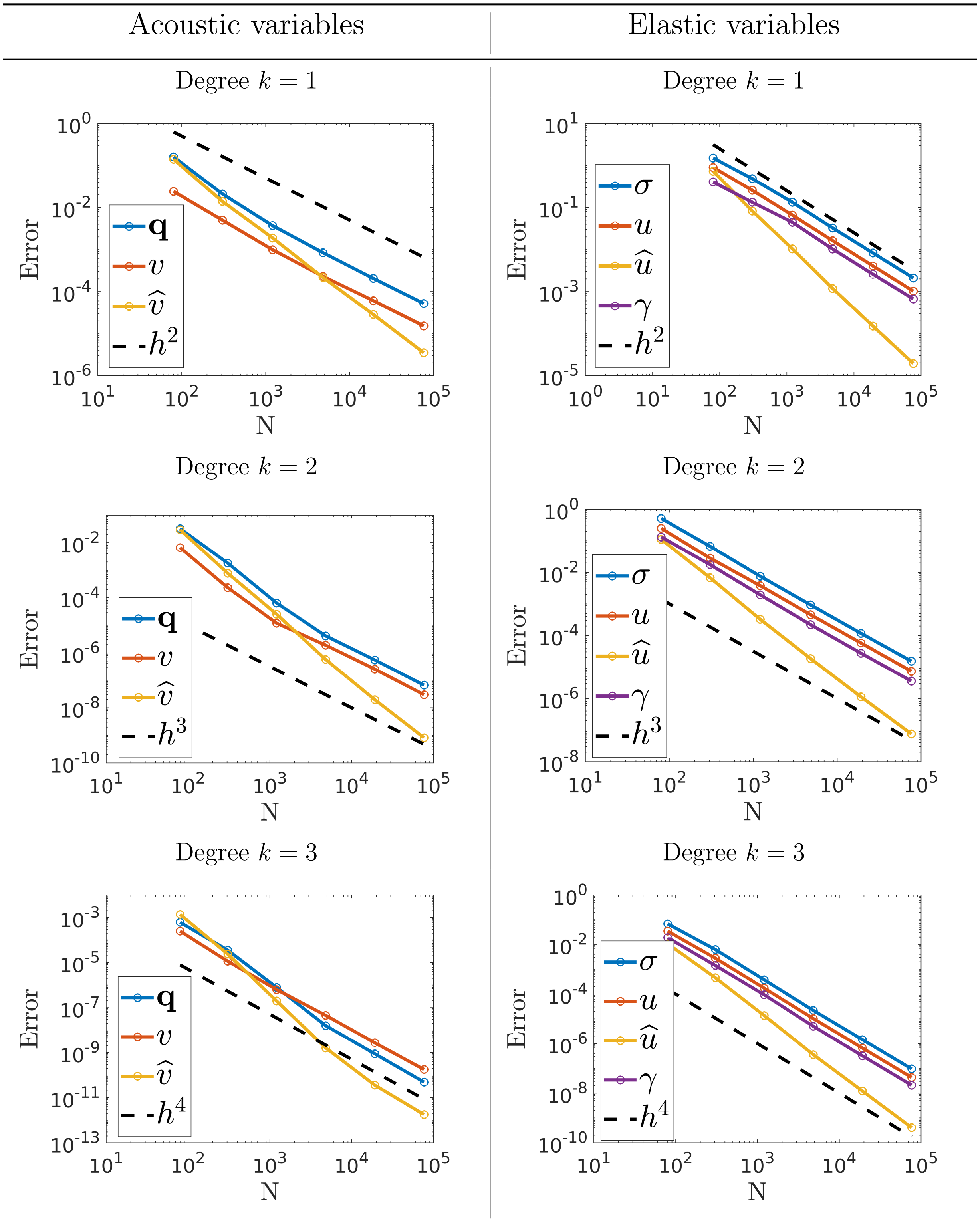

Figure 1.4: Discretization error as a function of the number of elements in the domain for the coupled acoustic/elastic problem. Acoustic variables are displayed on the first column and elastic variables on the second column.

Chapter 2

An Incursion in the Method of Fundamental Solutions

2.1 The Method of Fundamental Solutions

The Method of Fundamental Solutions (MFS) is a numerical method employed to solve boundary value problems for linear partial differential equations with a known fundamental solution. The solution to the problem is approximated as a linear combination of shifted fundamental solutions. Let us recall that if $\mathcal{L}$ is a linear partial differential operator, then Φ is called a fundamental solution if $\mathcal{L}\Phi = \delta$ in the sense of distributions, where δ stands for the Dirac delta distribution centered at the origin.

Due to the linearity of the operator, it follows that any linear combination of the form

$$u = \sum_{i=1}^{n} \alpha_i \Phi_{\boldsymbol{x}_i}, \tag{2.1}$$

where $\alpha_i \in \mathbb{R}$ and $\Phi_{\boldsymbol{x}_i} := \Phi(\cdot - \boldsymbol{x}_i)$ is the Green's function shifted to the point $\boldsymbol{x}_i$, would satisfy the PDE

$$\mathcal{L}u = 0 \qquad \text{in } \Omega \tag{2.2}$$

as long as $\boldsymbol{x}_i \notin \Omega$ for all $1 \leq i \leq n$. Therefore, if $\mathcal{B}$ is a linear operator imposing boundary conditions that guarantee well-posedness, it is possible to approximate the solution to boundary value problems of the form

$$\mathcal{L}u = 0 \quad \text{in } \Omega\,, \tag{2.3a}$$

$$\mathcal{B}u = g \quad \text{on } \partial\Omega\,, \tag{2.3b}$$

by choosing an ansatz of the form (2.1), and using the boundary condition (2.3b) to determine the locations $\boldsymbol{x}_i \in \Omega^c$ and the coefficients α_i that would make the approximation satisfy the problem (2.3) up to a predetermined tolerance.

The main idea is then to set some source points outside the domain, and force that a linear combination of those solutions satisfy the boundary condition at specific collocation points. This can be written as a linear system where the unknowns are the coefficients of the linear combination. Once the linear system has been solved, the solution and its derivatives can be evaluated directly at any point within the domain.

The MFS is a meshfree method that is very easy to implement and, in numerous cases, the error can reach machine precision. Nevertheless, this kind of method presents an —often called— "uncertainty principle" [1, 53]: you cannot get both accurate results and good conditioning.

The advent of the method gave rise to two distinct lines of development: the "fixed" one, in which the coefficients of the linear combination are the only unknowns —sometimes referred to as the Charge Simulation Method or the Method of Auxiliary Charges— and the "adaptive" one, which is based on simultaneously determining the mentioned coefficients and the coordinates of the source points through a nonlinear optimization problem. Both the adaptive method and some sophisticated modifications which have been proposed may be useful, but they directly weaken one of the most attractive features of the MFS: its simplicity.

One of the main challenges associated with the method pertains to the selection of the location of the sources. This has been the subject of study of numerous papers, e.g., [1, 11, 41, 42]. In the case of the Laplace and Helmholtz exterior problems with Dirichlet boundary conditions, if the data satisfies the equation (in which case it is called *harmonic* or *metaharmonic*, respectively), then the advice is to place the source points in a small circle near the center of the complement of the domain [17]. This case is particularly relevant when studying wave scattering problems. In this setting, the boundary data is assumed to come from an incident wave that interacts with an obstacle whose boundary is precisely the boundary of the PDE problem. In this setting, the physics of the problem dictate that the incident wave, providing the boundary data, must indeed be a solution to the PDE in free space.

On the contrary, when the data does not satisfy the equation, the recommendation is to place them in a curve with a shape similar to the boundary of the domain, with each source point situated at a specific distance from the corresponding boundary collocation point [11, 17, 42]. This distance can be changed to achieve more favorable outcomes, see [17, Example 8.1].

In what follows, we present some experiments that will help us to understand both the method itself and the results it produces.

- In Experiment I, we will see how to apply the method explicitly and present the results obtained when solving an exterior Helmholtz boundary value problem with metaharmonic Dirichlet data, i.e., when the data satisfies the Helmholtz equation.

- In Experiment II, we present the method applied to an exterior acoustic scattering problem.

We start by introducing some additional notation. Given $\boldsymbol{x} = (x, y) \in \mathbb{R}^2$ and $p \geq 1$, let us consider the usual vector p-norm

$$\|\boldsymbol{x}\|_p := (|x|^p + |y|^p)^{1/p}$$

(if $p = \infty$, then $\|\boldsymbol{x}\|_\infty := \max\{|x|, |y|\}$ is the Chebyshev norm) and the closed unit p-ball around the origin

$$B_p := \{\boldsymbol{x} \in \mathbb{R}^2 : \|\boldsymbol{x}\|_p \leq 1\}.$$

For $p \in [1, \infty)$, the boundary of these balls can be written as

$$B_p = \{(x, y) \in \mathbb{R}^2 : x = \operatorname{sign}(\cos\theta)|\cos\theta|^{2/p}, y = \operatorname{sign}(\sin\theta)|\sin\theta|^{2/p}, 0 \leq \theta \leq 2\pi\}.$$

2.2 Experiment I - Metaharmonic Data

This section is inspired in [17, Example 3]. Given a bounded obstacle $\Omega = B_p \subset \mathbb{R}^2$, $p \in \{10^2, 10^4, 10^6, \infty\}$, we are interested in solving the following boundary value problem for the Helmholtz equation

$$-\Delta u - \kappa^2 u = 0 \qquad \text{in } \mathbb{R}^2 \backslash \bar{\Omega}, \tag{2.4}$$

$$u = \frac{H_0^{(1)}\left(\kappa\sqrt{x^2 + y^2}\right)}{H_0^{(1)}(\kappa)} \qquad \text{on } \Gamma := \partial\Omega, \tag{2.5}$$

$$\partial_r u - i\kappa u = o\left(r^{-1/2}\right) \qquad \text{when } r = \|(x, y)\|_2 \to \infty, \tag{2.6}$$

where κ is the wavenumber, $H_0^{(1)}$ is the Hankel function of the first kind of order zero

$$H_0^{(1)}(\kappa r) = J_0(\kappa r) + iY_0(\kappa r),$$

J_0 and Y_0 are the Bessel functions of the first and second kind of order zero respectively, and (2.6) is the Sommerfeld radiation condition, which is needed for the well-posedness of the exterior problem. Physically, this condition ensures that only outgoing waves in the radial direction are admissible. The function

$$u_{ex} := \frac{H_0^{(1)}\left(\kappa\sqrt{x^2+y^2}\right)}{H_0^{(1)}(\kappa)}$$

appearing in the boundary condition (2.5) is in fact a solution to the Helmholtz equation (2.4) in free space, thus the Dirichlet data is metaharmonic.

Given $N \in \mathbb{N}$, we take N different values $\theta_j \in [0, 2\pi)$, $j \in \{1, \ldots, N\}$, and set the collocation points as

$$\boldsymbol{c}_j = \left(\operatorname{sign}(\cos\theta_j)|\cos\theta_j|^{2/p}, \operatorname{sign}(\sin\theta_j)|\sin\theta_j|^{2/p}\right), \quad j \in \{1, \ldots, N\}.$$

Choose the source points from a circumference of radius $R \in (0, 1)$ centered at the origin:

$$\boldsymbol{s}_j = (R\cos(\mu_j), R\sin(\mu_j)), \quad \text{where } \mu_j = \frac{2\pi(j-1)}{N}, \quad j \in \{1, \ldots, N\}.$$

In two dimensions, a fundamental solution of the Helmholtz equation satisfying the Sommerfeld radiation condition (2.6) is

$$\Phi(r) := \frac{i}{4} H_0^{(1)}(\kappa r),$$

with $r = \|(x, y)\|_2$. Then, for any $j \in \{1, \ldots, N\}$, the shifted fundamental solution $\Phi_{\boldsymbol{s}_j}(\|\cdot\|_2) = \Phi(\|\cdot - \boldsymbol{s}_j\|_2)$ verifies

$$\begin{aligned} -\Delta\Phi_{\boldsymbol{s}_j} - \kappa^2\Phi_{\boldsymbol{s}_j} &= 0 && \text{in } \mathbb{R}^2 \backslash \bar{\Omega}, \\ \partial_r\Phi_{\boldsymbol{s}_j} - i\kappa\Phi_{\boldsymbol{s}_j} &= o\left(r^{-1/2}\right) && \text{when } r = \|(x, y)\|_2 \to \infty. \end{aligned}$$

If we compare this with the exterior boundary value problem for Helmholtz (2.4) - (2.6), the only remaining condition to be satisfied is the boundary condition (2.5). For this purpose, we ask the linear combination

$$u_N = \sum_{l=1}^{N} \alpha_l \Phi_{\boldsymbol{s}_l}$$

to satisfy the boundary condition at least at the collocation points $\boldsymbol{c}_j$, for all $j \in \{1, \dots, N\}$. We can express this through the following square linear system of equations:

$$\begin{pmatrix} \Phi\left(\|\boldsymbol{c}_1 - \boldsymbol{s}_1\|_2\right) & \Phi(\|\boldsymbol{c}_1 - \boldsymbol{s}_2\|_2) & \cdots & \Phi(\|\boldsymbol{c}_1 - \boldsymbol{s}_N\|_2) \\ \Phi(\|\boldsymbol{c}_2 - \boldsymbol{s}_1\|_2) & \Phi(\|\boldsymbol{c}_2 - \boldsymbol{s}_2\|_2) & \cdots & \Phi(\|\boldsymbol{c}_2 - \boldsymbol{s}_N\|_2) \\ \vdots & \vdots & \ddots & \vdots \\ \Phi(\|\boldsymbol{c}_N - \boldsymbol{s}_1\|_2) & \Phi(\|\boldsymbol{c}_N - \boldsymbol{s}_2\|_2) & \cdots & \Phi(\|\boldsymbol{c}_N - \boldsymbol{s}_N\|_2) \end{pmatrix} \begin{pmatrix} \alpha_1 \\ \alpha_2 \\ \vdots \\ \alpha_N \end{pmatrix} = \begin{pmatrix} \dfrac{H_0^{(1)}(\kappa\|\boldsymbol{c}_1\|_2)}{H_0^{(1)}(\kappa)} \\ \vdots \\ \dfrac{H_0^{(1)}(\kappa\|\boldsymbol{c}_N\|_2)}{H_0^{(1)}(\kappa)} \end{pmatrix}.$$

Note that there is no guarantee about the invertibility of the matrix. We will solve this linear system with MATLAB's \ command, even in the cases when the matrix is singular. To compute the evaluations of the function $H_0^{(1)}$ we use the command BESSELH.

The usual ways of measuring error when applying the MFS in these types of problems are the normalized root mean square (RMS) error,

$$E_{\text{rms}} := \frac{\sqrt{\dfrac{1}{N_e}\displaystyle\sum_{m=1}^{N_e} \left(\operatorname{Re}(u_{ex}(\boldsymbol{e}_m) - u_N(\boldsymbol{e}_m))\right)^2}}{\max\{\operatorname{Re}(u_{ex}(\boldsymbol{e}_m))\} - \min\{\operatorname{Re}(u_{ex}(\boldsymbol{e}_m))\}},$$

and the normalized maximum error,

$$E_{\max}^{\text{bd}} := \frac{\max\{|\operatorname{Re}(u_{ex}(\boldsymbol{e}_m) - u_N(\boldsymbol{e}_m))|\}}{\max\{\operatorname{Re}(u_{ex}(\boldsymbol{e}_m))\} - \min\{\operatorname{Re}(u_{ex}(\boldsymbol{e}_m))\}},$$

where $\{\boldsymbol{e}_m\}_{m=1}^{N_e} \subset \Gamma$ is a set of error sampling points such that $\{\boldsymbol{e}_m\}_{m=1}^{N_e} \cap \{\boldsymbol{c}_j\}_{j=1}^{N} = \emptyset$. Let us choose $N_e \approx 10N$. In this experiment, we know the exact solution not only in the boundary of the obstacle but also in all $\mathbb{R}^2 \backslash \bar{\Omega}$, so we can measure the error wherever we want. Thus, we will also calculate a normalized maximum error

$$E_{\max}^{\text{sq}} := \frac{\max\{|\operatorname{Re}(u_{ex}(\boldsymbol{g}_n) - u_N(\boldsymbol{g}_n))|\}}{\max\{\operatorname{Re}(u_{ex}(\boldsymbol{g}_n))\} - \min\{\operatorname{Re}(u_{ex}(\boldsymbol{g}_n))\}},$$

where $\boldsymbol{g}_n$ are some predetermined evaluation points. In this case, we will consider a regular grid of the square $[-8, 8]^2$, with points separated horizontally and vertically by a distance $h = 0.025$. The evaluation points $\boldsymbol{g}_n$ are all the points on the grid that fall outside the obstacle

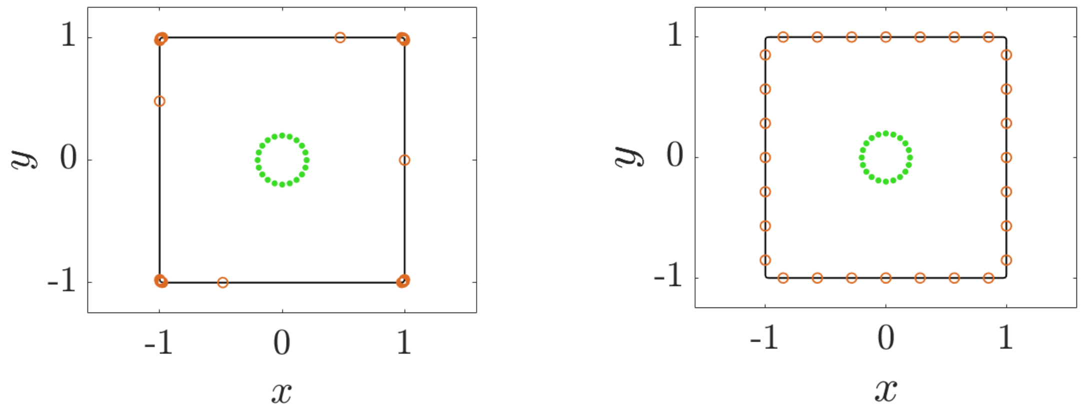

Figure 2.1: Location of collocation (○) and source (•) points on $\Omega = B_{10^2}$, with $N = 28$ and $R = 0.2$. On the left: the collocation points are very close to each other at the corners because of the choice of uniformly distributed θ_j. On the right: the collocation points obtained with our routine.

Ω. Note that we distinguish the normalized maximum errors by their superscripts: $^{\text{bd}}$ stands for "boundary" and $^{\text{sq}}$, for "square".

Due to the parametrization, if we take $\theta_j = \dfrac{2\pi(j-1)}{N}, j \in \{1, \ldots, N\}$, the collocation points would be very close to each other at the corners of the domain (see the left-hand side of Figure 2.1). In order to distribute the collocation points evenly around Γ, we have implemented a MATLAB routine (see the right-hand side of Figure 2.1).

Let us solve the exterior Helmholtz boundary value problem (2.4) - (2.6) numerically by applying the MFS in sixteen different configurations: taking $\kappa = 10$, four problems ($p \in \{10^2, 10^4, 10^6, \infty\}$) will be computed for four different radii ($R \in \{0.2, 0.4, 0.6, 0.8\}$).

In Table 2.1, we show the results obtained for $N = 28$ and $\kappa = 10$. Notice that as R grows from 0.2 to 0.8 the results become less and less accurate. Thus, we have confirmed the recommendation to place the source points on a circumference with small radius. Also, we can conclude that in this experiment it did not matter how sharp the domain was, since practically the same results were obtained for all four figures: from B_{10^2} to the square B_∞.

In Figure 2.2, we compare in more detail the experiments performed with B_{10^2} for several values of N, with $R = 0.2$ on the left and $R = 0.8$ on the right. The first row of images shows the error incurred by the MFS as N increased. Note that for $R = 0.2$ only twenty points were

p	R	E_{rms}	$E_{\max}^{\text{bd}}$	$E_{\max}^{\text{sq}}$	p	R	E_{rms}	$E_{\max}^{\text{bd}}$	$E_{\max}^{\text{sq}}$
10^2	0.2	6.93e−16	2.28e−15	5.47e−15	10^4	0.2	5.45e−16	1.60e−15	5.60e−15
	0.4	1.93e−13	6.70e−13	1.57e−12		0.4	1.91e−13	6.67e−13	1.56e−12
	0.6	3.61e−08	1.25e−07	2.95e−07		0.6	3.58e−08	1.24e−07	2.93e−07
	0.8	7.71e−05	2.67e−04	6.26e−04		0.8	7.65e−05	2.65e−04	6.22e−04
10^6	0.2	6.50e−16	1.84e−15	5.63e−15	∞	0.2	5.10e−16	1.60e−15	5.60e−15
	0.4	1.91e−13	6.67e−13	1.56e−12		0.4	1.91e−13	6.67e−13	1.56e−12
	0.6	3.58e−08	1.25e−07	2.93e−07		0.6	3.58e−08	1.25e−07	2.93e−07
	0.8	7.65e−05	2.65e−04	6.22e−04		0.8	7.65e−05	2.65e−04	6.22e−04

Table 2.1: Results obtained varying the domain and the radius of the circle of sources, with $N = 28$ and $\kappa = 10$.

enough to obtain errors close to 10^{-15}, while for $R = 0.8$ it only reaches 10^{-6} with sixty points. In the second row, we can see the absolute error of the real part of the solution when we take twenty-eight collocation and twenty-eight source points. It is interesting to realize that the error is accumulated near the midpoints of the domain sides when $R = 0.8$. This is due the proximity of the source points to the collocation points in those parts (see Figure 2.3). The third row presents the condition number of the matrices for the different values of N with which the experiment was performed. For the smaller radius, the condition number grows extremely fast as the number of point increases, while for $R = 0.8$ the number also grows but not as much as in the other case. Combining the information provided by the plots in the first and third row, we can clearly observe the aforementioned uncertainty principle. Finally, the fourth row of Figure 2.2 shows the rank of the matrices in each case, where the dotted line indicates the full rank matrices.

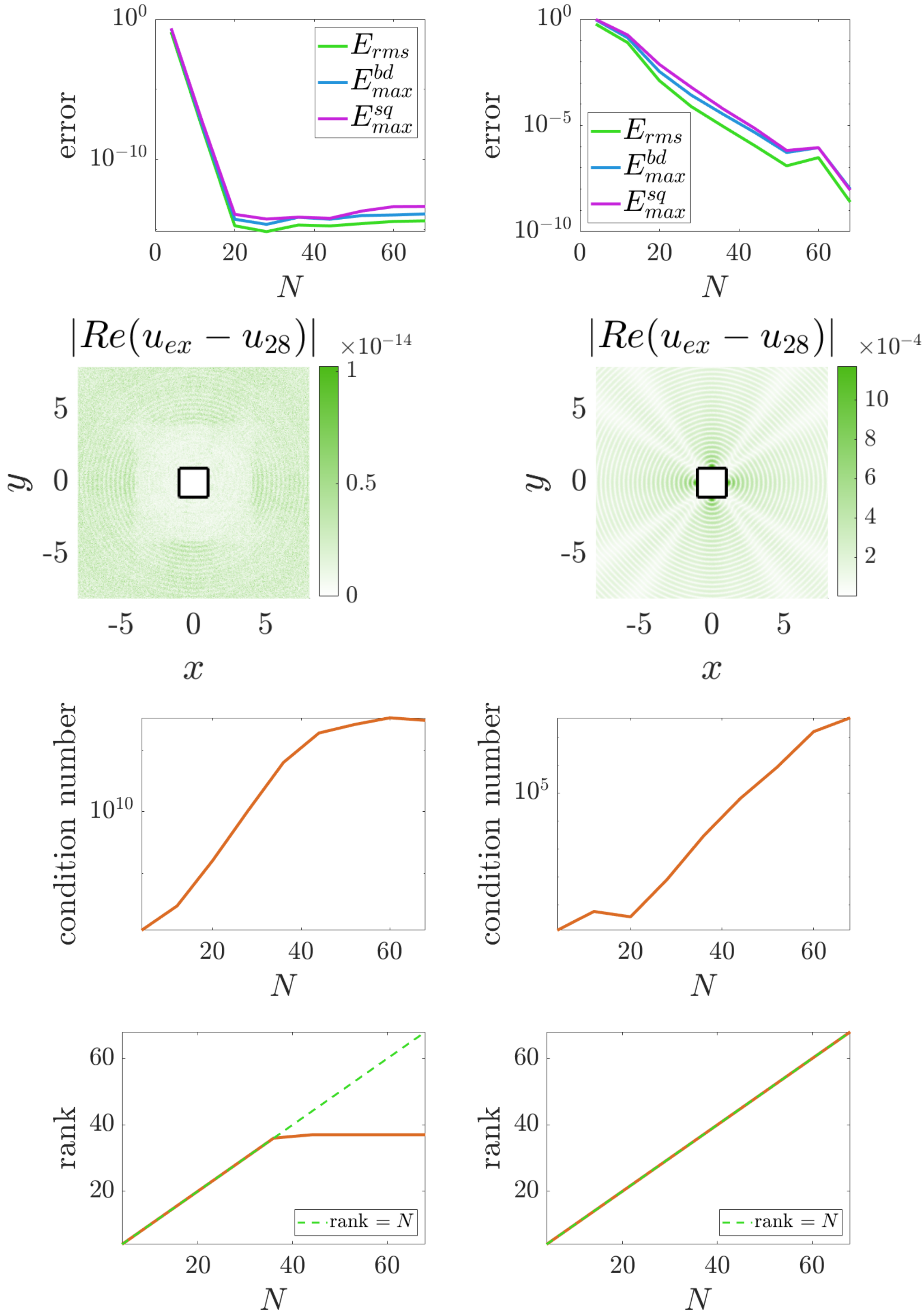

Figure 2.2: Results for $\kappa = 10$ and $p = 10^2$. $R = 0.2$ (left) and $R = 0.8$ (right).

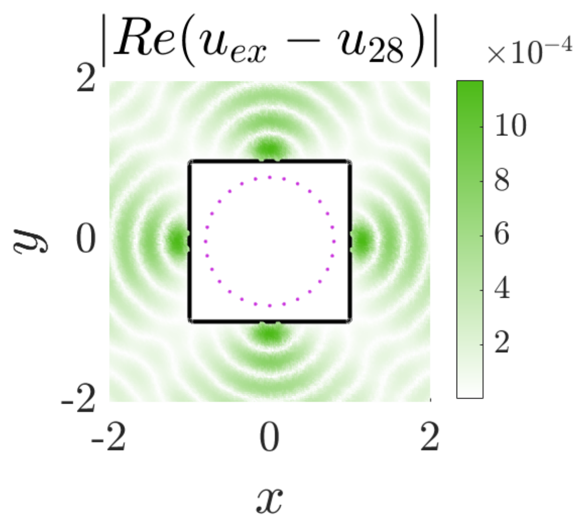

Figure 2.3: Zoom to the graph on the right in the second row of Figure 2.2. The source points are represented by •.

2.3 Experiment II - Acoustic Scattering

Now, let us simulate an acoustic scattering problem using the Method of Fundamental Solutions. We are interested in the problem

$$-\Delta u - \kappa^2 u = 0 \qquad \text{in } \mathbb{R}^2 \backslash \bar{\Omega}, \tag{2.7}$$

$$u = -e^{i\kappa \boldsymbol{d}\cdot(x,y)} \qquad \text{on } \Gamma := \partial\Omega, \tag{2.8}$$

$$\partial_r u - i\kappa u = o\left(r^{-1/2}\right) \qquad \text{when } r = \|(x,y)\|_2 \to \infty, \tag{2.9}$$

where the incident wave is $u^{\text{inc}} = e^{i\kappa \boldsymbol{d}\cdot(x,y)}$ and $\boldsymbol{d}$ is the propagation direction. Taking $\Omega = B_2$ and $\boldsymbol{d} = 2^{-1/2}(1,1)$, and placing the source points in a circle of radius 0.3 centered at the origin, we obtain the results shown in Figure 2.4, for $\kappa = 10$ and $N = 524$.

Note that the solution makes physical sense, since the wave hits the object and scatters, leaving a white shadow behind the scatterer. However, we obtain an error $E_{\text{rms}} = 1.1e-03$ at the boundary. So, it is also future work to investigate how this approximation can be improved.

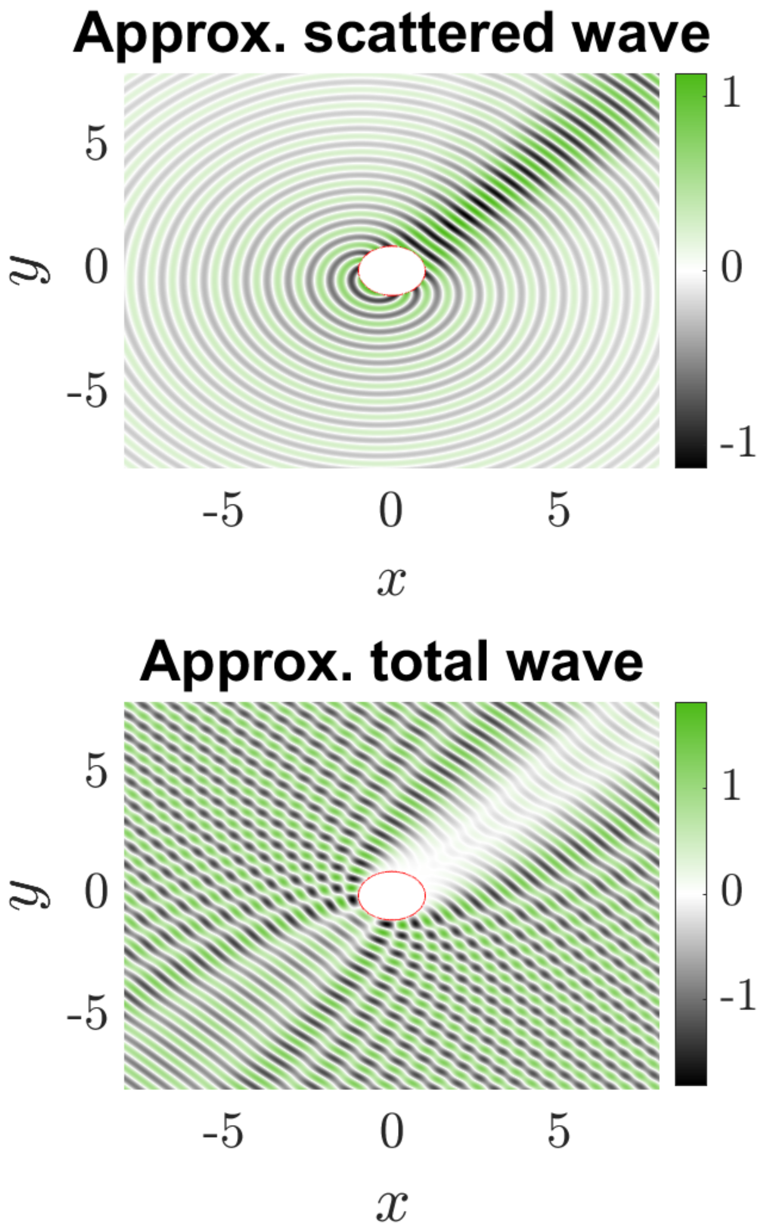

Figure 2.4: Approximate scattered wave (top) and approximate total wave (bottom).

Conclusions and Future Work

Let us summarize the main contributions of this work and give a brief description of eventual future works.

2.4 Conclusions

Upon the results presented in the first chapter of this thesis, we can arrive to the following conclusions:

- We have proposed and analyzed a coupled HDG scheme for the interaction between acoustic and elastic waves in the Laplace domain, proving that the scheme has a unique solution.
- Using a polynomial degree of k in the local spaces, we have showed that the errors in the unknowns $\boldsymbol{\sigma}, \boldsymbol{u}, \boldsymbol{\gamma}, \boldsymbol{q}$ and v converge with optimal order $k+1$.

According to the results presented in the second chapter of this work:

- We have learned about the Method of Fundamental Solutions, showing that it works incredibly well for problems like Experiment I.
- We have confirmed the advice given in the literature about the location of the source points for boundary value problems with metaharmonic data. In addition, we were able to empirically confirm the so-called uncertainty principle for the MFS.

- We have been aware of how sensitive the method is with respect to the location of source points, which makes sense considering the number of papers dealing with this topic.

2.5 Future work

From the development of this work, we have been able to find several directions for future work:

- Since we already have the HDG codes for elasticity and acoustics, it remains to implement the coupled scheme by linking the two programs.
- To study some modifications of the Method of Fundamental Solutions to try to obtain better approximations for the acoustic scattering problem.
- To develop the coupling of the Method of Fundamental Solutions with the Hybridizable Discontinuous Galerkin scheme in order to solve the problem in the unbounded domain.

Bibliography

[1] C. J. Alves. On the choice of source points in the method of fundamental solutions. *Engineering Analysis with Boundary Elements*, 33(12):1348–1361, 2009.

[2] C. J. S. Alves and P. R. S. Antunes. Wave scattering problems in exterior domains with the method of fundamental solutions. *Numerische Mathematik*, 156(2):375–394, Feb. 2024.

[3] R. Araya, R. Rodríguez, and P. Venegas. Numerical analysis of a time domain elastoacoustic problem. *IMA Journal of Numerical Analysis*, 40(2):1122–1153, 01 2019.

[4] I. Bermúdez, J. Manríquez, and M. Solano. A hybridizable discontinuous Galerkin method for Stokes/Darcy coupling on dissimilar meshes. *IMA J. Numer. Anal.*, 2025.

[5] T. S. Brown, T. Sánchez-Vizuet, and F.-J. Sayas. Evolution of a semidiscrete system modeling the scattering of acoustic waves by a piezoelectric solid. *ESAIM: Mathematical Modeling and Numerical Analysis (M2AN)*, 52(2):423–455, 2018. (arXiv:1612.04063).

[6] R. Bustinza, B. López-Rodríguez, and M. Osorio. An a priori error analysis of an HDG method for an eddy current problem. *Mathematical Methods in the Applied Sciences*, 41(7):2795–2810, 2018.

[7] L. Camargo, B. López-Rodríguez, M. Osorio, and M. Solano. An HDG method for Maxwell's equations in heterogeneous media. *Computer Methods in Applied Mechanics and Engineering*, 368:113178, 2020.

[8] J. M. Cárdenas and M. Solano. A high order unfitted hybridizable discontinuous Galerkin method for linear elasticity. *IMA Journal of Numerical Analysis*, 44(2):945–979, 05 2023.

[9] A. Cesmelioglu, B. Cockburn, N. C. Nguyen, and J. Peraire. Analysis of HDG methods for Oseen equations. *J. Sci. Comput.*, 55(2):392–431, May 2013.

[10] A. Cesmelioglu, B. Cockburn, and W. Qiu. Analysis of a hybridizable discontinuous Galerkin method for the steady-state incompressible Navier–Stokes equations. *Math. Comp.*, 86(306):1643–1670, 2017.

[11] C. S. Chen, A. Karageorghis, and Y. Li. On choosing the location of the sources in the MFS. *Numerical Algorithms*, 72(1):107–130, 2016.

[12] H. Chen, P. Lu, and X. Xu. A hybridizable discontinuous Galerkin method for the Helmholtz equation with high wave number. *SIAM Journal on Numerical Analysis*, 51(4):2166–2188, 2013.

[13] H. Chen, W. Qiu, and K. Shi. A priori and computable a posteriori error estimates for an HDG method for the coercive Maxwell equations. *Computer Methods in Applied Mechanics and Engineering*, 333:287 – 310, 2018.

[14] H. Chen, W. Qiu, K. Shi, and M. Solano. A superconvergent HDG method for the Maxwell equations. *Journal of Scientific Computing*, 70(3):1010–1029, 2017.

[15] Y. Chen and B. Cockburn. Analysis of variable-degree HDG methods for convection-diffusion equations. Part I: general nonconforming meshes. *IMA Journal of Numerical Analysis*, 32(4):1267–1293, Feb. 2012.

[16] Y. Chen and B. Cockburn. Analysis of variable-degree HDG methods for convection-diffusion equations. part II: Semimatching nonconforming meshes. *Mathematics of Computation*, 83(285):87–111, May 2013.

[17] A. H. Cheng and Y. Hong. An overview of the method of fundamental solutions — Solvability, uniqueness, convergence, and stability. *Engineering Analysis with Boundary Elements*, 120:118–152, 2020.

[18] B. Cockburn, J. Gopalakrishnan, and J. Guzmán. A new elasticity element made for enforcing weak stress symmetry. *Mathematics of Computation*, 79(271):1331–1349, 2010.

[19] B. Cockburn, J. Gopalakrishnan, and R. Lazarov. Unified hybridization of discontinuous Galerkin, mixed, and continuous Galerkin methods for second order elliptic problems. *SIAM J. Numer. Anal.*, 47(2):1319–1365, 2009.

[20] B. Cockburn, J. Gopalakrishnan, N. C. Nguyen, J. Peraire, and F.-J. Sayas. Analysis of HDG methods for Stokes flow. *Math. Comp.*, 80:723–760, 2011.

[21] B. Cockburn, J. Gopalakrishnan, and F.-J. Sayas. A projection-based error analysis of HDG methods. *Mathematics of Computation*, 79(271):1351–1367, Mar. 2010.

[22] B. Cockburn, W. Qiu, and M. Solano. A priori error analysis for HDG methods using extensions from subdomains to achieve boundary conformity. *Mathematics of Computation*, 83, 03 2014.

[23] B. Cockburn and K. Shi. Superconvergent HDG methods for linear elasticity with weakly symmetric stresses. *IMA Journal of Numerical Analysis*, 33(3):747–770, 10 2012.

[24] B. Cockburn and M. Solano. Solving Dirichlet boundary-value problems on curved domains by extensions from subdomains. *SIAM Journal on Scientific Computing*, 34(1):A497–A519, 2012.

[25] C. Domínguez, G. N. Gatica, and S. Meddahi. A posteriori error analysis of a fully-mixed finite element method for a two-dimensional fluid-solid interaction problem. *Journal of Computational Mathematics*, 33(6):606–641, 2015.

[26] B. Engquist and A. Majda. Absorbing boundary conditions for the numerical simulation of waves. *Mathematics of Computation*, 31(139):629–651, 1977.

[27] X. Feng, P. Lu, and X. Xu. A hybridizable discontinuous Galerkin method for the time-harmonic Maxwell equations with high wave number. *Computational Methods in Applied Mathematics*, 16(3):429–445, 2016.

[28] G. Fu, Y. Jin, and W. Qiu. Parameter-free superconvergent $H(\mathrm{div})$-conforming HDG methods for the Brinkman equations. *arXiv:1607.07662 [math.NA]*, July 2016.

[29] G. Fu, W. Qiu, and W. Zhang. An analysis of HDG methods for convection–dominated diffusion problems. *ESAIM: M2AN*, 49(1):225–256, 2015.

[30] G. N. Gatica, N. Heuer, and S. Meddahi. Coupling of mixed finite element and stabilized boundary element methods for a fluid–solid interaction problem in 3d. *Numerical Methods for Partial Differential Equations*, 30(4):1211–1233, 2014.

[31] G. N. Gatica, A. Márquez, and S. Meddahi. Analysis of the coupling of lagrange and arnold-falk-winther finite elements for a fluid-solid interaction problem in three dimensions. *SIAM Journal on Numerical Analysis*, 50(3):1648–1674, 2012.

[32] G. N. Gatica and F. A. Sequeira. A priori and a posteriori error analyses of an augmented HDG method for a class of quasi-Newtonian Stokes flows. *J. Sci. Comput.*, 69:1192–1250, 2016.

[33] G. N. Gatica and F. A. Sequeira. Analysis of the HDG method for the Stokes–Darcy coupling. *Numer. Methods Partial Differential Equations*, 33(3):885–917, 2017.

[34] R. Griesmaier and P. Monk. Error analysis for a hybridizable discontinuous Galerkin method for the Helmholtz equation. *Journal of Scientific Computing*, 49(3):291–310, 2011.

[35] J. Guzmán. A unified analysis of several mixed methods for elasticity with weak stress symmetry. *Journal of Scientific Computing*, 44:156–169, 2010.

[36] L. Halpern and L. N. Trefethen. Wide-angle one-way wave equations. *The Journal of the Acoustical Society of America*, 84(4):1397–1404, 10 1988.

[37] R. L. Higdon. Numerical absorbing boundary conditions for the wave equation. *Mathematics of Computation*, 49(179):65–90, 1987.

[38] G. C. Hsiao and T. Sánchez-Vizuet. Time-dependent wave-structure interaction revisited: Thermo-piezoelectric scatterers. *Fluids*, 6(3), 2021. (arXiv: 2102.04118).

[39] G. C. Hsiao, T. Sánchez-Vizuet, and F.-J. Sayas. Boundary and coupled boundary-finite element methods for transient wave-structure interaction. *IMA Journal of Numerical Analysis*, 37(1):237–265, 2016. (arXiv:1509.01713).

[40] L. N. T. Huynh, N. C. Nguyen, J. Peraire, and B. C. Khoo. A high-order hybridizable discontinuous Galerkin method for elliptic interface problems. *International Journal for Numerical Methods in Engineering*, 93(2):183–200, jan 2013.

[41] A. Karageorghis. A practical algorithm for determining the optimal pseudo-boundary in the method of fundamental solutions. *Advances in Applied Mathematics and Mechanics*, 1(4):510–528, 2009.

[42] M. Li, C. Chen, and A. Karageorghis. The MFS for the solution of harmonic boundary value problems with non-harmonic boundary conditions. *Computers & Mathematics with Applications*, 66(11):2400–2424, 2013.

[43] Q.-H. Liu and J. Tao. The perfectly matched layer for acoustic waves in absorptive media. *The Journal of the Acoustical Society of America*, 102(4):2072–2082, 10 1997.

[44] J. Manríquez, N.-C. Nguyen, and M. Solano. A dissimilar non-matching HDG discretization for Stokes flows. *Comput. Methods Appl. Mech. Engrg.*, 399:Paper No. 115292, 30, 2022.

[45] S. Meddahi, D. Mora, and R. Rodríguez. Finite element analysis for a pressure–stress formulation of a fluid–structure interaction spectral problem. *Computers & Mathematics with Applications*, 68(12, Part A):1733–1750, 2014.

[46] N. C. Nguyen, J. Peraire, and B. Cockburn. An implicit high–order hybridizable discontinuous Galerkin method for linear convection–diffusion equations. *J. Comput. Phys.*, 228(9):3232–3254, 2009.

[47] N. C. Nguyen, J. Peraire, and B. Cockburn. Hybridizable discontinuous Galerkin methods for the time-harmonic Maxwell's equations. *Journal of Computational Physics*, 230(19):7151–7175, 2011.

[48] N. C. Nguyen, J. Peraire, and B. Cockburn. An implicit high-order hybridizable discontinuous Galerkin method for the incompressible Navier–Stokes equations. *J. Comput. Phys.*, 230(4):1147–1170, 2011.

[49] W. Qiu, J. Shen, and K. Shi. HDG method for linear elasticity with strong symmetric stresses. *Mathematics of Computations*, 87:69–93, 2018.

[50] N. Sánchez, T. Sánchez-Vizuet, and M. E. Solano. Afternote to "Coupling at a Distance": Convergence analysis and a priori error estimates. *Computational Methods in Applied Mathematics*, 22(4):945–970, 2022.

[51] T. Sánchez-Vizuet. *Integral and coupled integral-volume methods for transient problems in wave-structure interaction*. Phd thesis, University of Delaware, Newark, DE, 2016. Available at https://udspace.udel.edu/items/88d8c2c7-633a-456c-90b7-4a7a60ca7317.

[52] T. Sánchez-Vizuet. A symmetric boundary integral formulation for time-domain acoustic-elastic scattering. *(Submitted)*, 2025. arXiv:2502.04767.

[53] R. Schaback. Error estimates and condition numbers for radial basis function interpolation. *Advances in Computational Mathematics*, 3(3):251–264, 1995.

[54] M. Solano, S. Terrana, N.-C. Nguyen, and J. Peraire. An HDG method for dissimilar meshes. *IMA J. Numer. Anal.*, 42(2):1665–1699, 2022.

[55] L. N. Trefethen and L. Halpern. Well-posedness of one-way wave equations and absorbing boundary conditions. *Mathematics of Computation*, 47(176):421–435, 1986.

[56] B. Wang and B. C. Khoo. Hybridizable discontinuous Galerkin method (HDG) for Stokes interface flow. *Journal of Computational Physics*, 247:262–278, Aug. 2013.

[57] B. Zhu and H. Wu. Preasymptotic error analysis of the HDG method for Helmholtz equation with large wave number. *Journal of Scientific Computing*, 87(2):1–34, 2021.